SIAM REVIEW
Vol. 51, No. 3, pp. 501–542

Vortex Lattice Theory: A Particle Interaction Perspective*

Paul K. Newton†
George Chamoun†

Abstract. Recent experiments on the formation of vortex lattices in Bose–Einstein condensates has produced the need for a mathematical theory that is capable of predicting a broader class of lattice patterns, ones that are free of discrete symmetries and can form in a random environment. We give an overview of an N-particle based Hamiltonian theory which, if formulated in terms of the $O(N^2)$ interparticle distances, leads to the analysis of a nonnormal "configuration" matrix whose nullspace structure determines the existence or nonexistence of a lattice. The singular value decomposition of this matrix leads to a method in which *all* lattice patterns and the associated particle strengths, in principle, can be classified and calculated by a random-walk scheme which systematically uses the m smallest singular values as a ratchet mechanism to home in on lattices with m-dimensional nullspaces, where $0 < m \leq N$. The resulting distribution of singular values encodes detailed geometric properties of the lattice and allows us to identify and calculate important quantitative measures associated with each lattice, including its size (as measured by the Frobenius or 2-norms), distance between the lattices (hence lattice density), robustness, and Shannon entropy as a quantitative measure of its level of disorder. This article gives an overview of vortex lattice theory from 1957 to the present, highlighting recent experiments in Bose–Einstein condensate systems and formulating questions that can be addressed by understanding the singular value decomposition of the configuration matrix. We discuss some of the computational challenges associated with producing large N lattices, the subtleties associated with understanding and exploiting complicated Hamiltonian energy surfaces in high dimensions, and we highlight ten important directions for future research in this area.

Key words. Abrikosov lattices, Bose–Einstein condensates, singular value decomposition, Brownian ratchets, Shannon entropy, random-walk schemes, Thomson's problem, mesh generation, Kullback–Leibler divergence

AMS subject classifications. 70F10, 76B47, 15A18, 37J99

DOI. 10.1137/07068597X

1. Introduction.

The modern theory of vortex lattices began in 1957 with the prediction by Abrikosov of the existence of triangular structures in what was then a new class of superconductor, called "superconductors of the second group," now called type II superconductors (Abrikosov (1957)). His prediction was an outgrowth of the newly developed theory of superconductivity by Ginzburg and Landau (1950) in which they used a wave function as their "order parameter" to study the superconducting phase transition. Abrikosov wondered what would happen when the "Ginzburg–Landau" parameter exceeded the critical value $1/\sqrt{2}$, in which case the surface energy

*Received by the editors March 21, 2007; accepted for publication (in revised form) March 5, 2008; published electronically August 5, 2009. The work was supported in part by grant NSF-DMS0504308.
http://www.siam.org/journals/sirev/51-3/68597.html

†Departments of Aerospace & Mechanical Engineering and Mathematics, Viterbi School of Engineering, University of Southern California, Los Angeles, CA 90089-1191 (newton@usc.edu, chamoun@usc.edu).

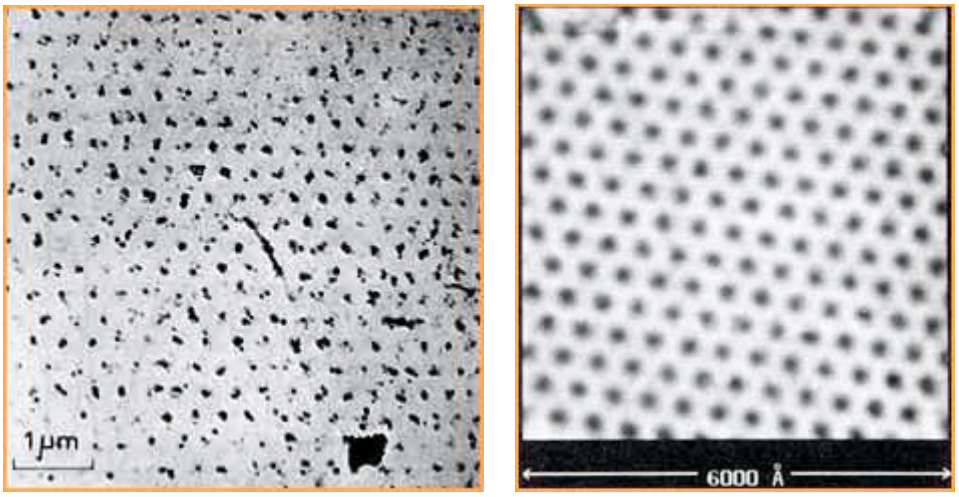

(a) (b)

Fig. 1.1 (a) *The first direct image of an "Abrikosov" triangular lattice in a type* II *superconductor from Essmann and Trauble* (1967) *(reprinted with permission from Elsevier). Each dark spot is a lattice site created by a nearly straight magnetic flux tube in a periodic arrangement, penetrating the specimen parallel to the applied field, with a diameter that is small compared to the lattice spacing.* (b) *The image of an "Abrikosov" triangular lattice in* $NbSe_2$ *using a scanning-tunneling microscope from Hess et al.* (1989) *(reprinted with permission from APS). The lattice is far more regular than previously imaged, and contains detail over a wider range of scales.*

of the material becomes negative. He predicted it would be possible for the material to produce periodic arrays of aligned magnetic flux tubes, with quantized values, penetrating the specimen parallel to the applied magnetic field. He also argued that the geometric configuration which would minimize the free energy of the system, in an isotropic medium, should be triangular.[1] Higher energy configurations, such as square or hexagonal lattices, should be possible in substances with crystalline symmetries that would "impose" these symmetries on the lattice and, ironically, it is the square lattice that Abrikosov shows in his 1957 publication, despite the fact that triangular lattices are now most associated with his name. Interestingly, his prediction, first made in 1953, did not create much of a stir since Landau and others did not believe in the possibility of a vortex lattice incommensurable with the crystalline structure which supports it (see the recollections in Abrikosov's Nobel lecture (2004)). However, after Feynman's (1955) publication on vortex tubes in superfluid helium with quantized circulations $\Gamma = \hbar/m$ ($\sim 0.001\text{cm}^2/\text{s}$), where $\hbar$ is Planck's constant and m is the mass of the ^{4}He atom, the idea seemed more palatable. As was remarked on in Aref et al. (2003), the association between Planck's constant and the vortex circulations, along with the fact that the rotational frequency of the lattice can be calculated from knowledge of the lattice pattern, implies that, in principle, Planck's constant (a microscopic quantity) can be calculated given sufficiently accurate measurements of macroscopic quantities, an intriguing but currently impractical possibility. The first direct image of such an "Abrikosov" lattice by Essmann and Trauble (1967) (see Figure 1.1(a), later using scanning-tunneling microscope imaging (see Figure 1.1(b))

[1] Triangular lattices have better stability properties than others, as shown in Fetter, Hohenberg, and Pincus (1966).

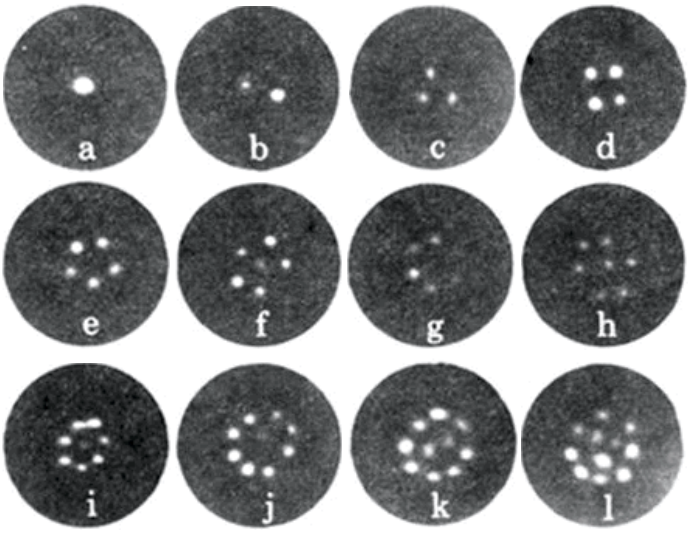

Fig. 1.2 *First good examples, after Yarmchuck, Gordon, and Packard* (1979) *(reprinted with permission from APS) of vortex lattice patterns in superfluid helium with* $1, \ldots, 11$ *vortices (light spots). The pattern is rotating with a predictable frequency based on the geometric properties of the pattern and the circulations are quantized and all equal.*

by Hess et al. (1989), and in superfluid helium by Yarmchuck, Gordon, and Packard (1979) (see Figure 1.2), ushered in the modern era of vortex lattice research that has flourished for the past 50 years and continues unabated. Recently, because of a new class of experiments, unprecedented in their microscopic detail, performed on more general lattices (not necessarily periodic) in Bose–Einstein condensate systems, this classical and fascinating subject has been reinvigorated and has produced the need for the development of a more comprehensive theory.

A good example of the type of imaging detail now available for these systems is shown in Figure 1.3 taken from Abo-Shaer et al. (2001) and Figure 1.4 taken from Engels et al. (2002). Figure 1.3 shows a sampling of vortex lattice patterns with 16, 32, 80, and 130 vortices. In these experiments, a collection of boson particles is trapped in an external potential, cooled to temperatures near absolute zero, which causes the atoms to collapse to the lowest quantum state of the external potential and exhibit quantum effects which collectively are visible on macroscopic scales (see Butts and Rokhar (1999)). Laser stirring then introduces angular momentum to the sample which manifests itself in the form of discrete quantized, nearly parallel vortex filaments. The higher the speed of rotation, the larger the number of vortices produced (since the rotation speed is a simple function of the total vortex strength of the collection of particles). Figure 1.4 shows both the front and side views of the lattice in order to document its two-dimensionality, as evidenced by the parallel vortex tubes shown from the sides, as well as its regularity, as seen by the nearly equal spacing of the peaks across a horizontal cut. The lattices can now be manipulated to a high degree by stressing the patterns, as shown, for example, in Figure 1.5, in which the size and shape of a basic cell can be altered, and defect patterns such as the line and grain boundary defects shown in Figure 1.6 can be produced routinely.

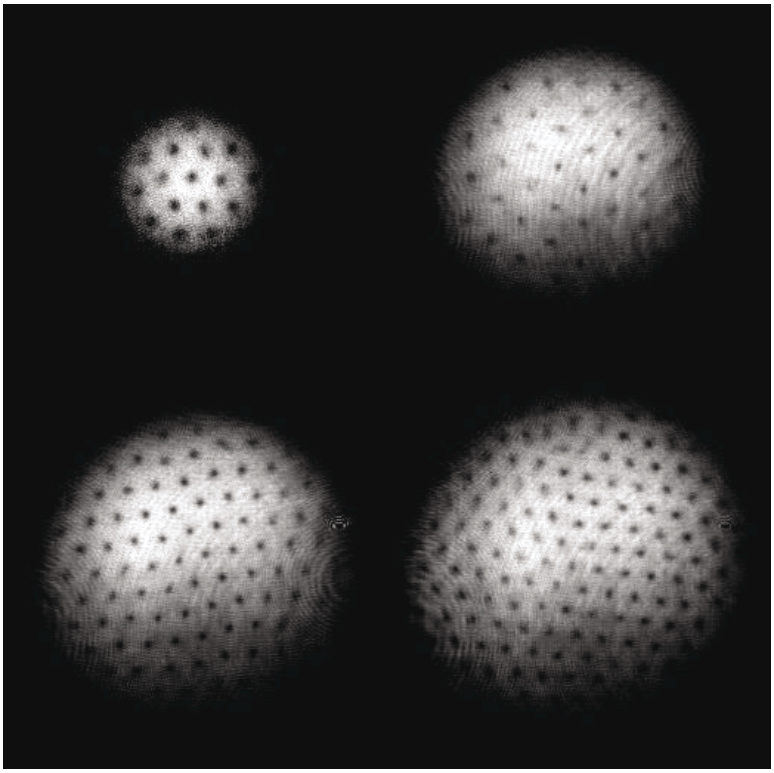

Fig. 1.3 *First good examples, from Abo-Shaer et al.* (2001) *(reprinted with permission from AAAS), of vortex lattice patterns in Bose–Einstein condensates with* 16*,* 32*,* 80*, and* 130 *vortices (dark spots) as the speed of rotation of the condensate is increased, crystallized in a triangular pattern. The diameter of the cloud in the last image is approximately* 1*mm.*

A fascinating precursor to the modern theory was conceived of by William Thomson (Lord Kelvin), who formulated his now defunct "vortex atom" theory of matter in the 1860s (Thomson (1867)), following Helmholtz' landmark 1858 study of vortex motion.[2] According to this view, and in his attempt to understand Faraday's magneto-optic rotation (1846), the underpinnings of matter were made up of atoms, which were thought of as loci of rotational motion embedded within a homogeneous ether pervading space. The "permanence" of these inviscid rotational structures, linked together in complex stable arrangements of rings and knots, were thought to give rigidity to matter and endow it with properties associated with the underlying vortex structures. In a letter to Helmholtz of 1867, Kelvin wrote:

> If there is a perfect fluid all through space, constituting the substance of all matter, a vortex-ring would be as permanent as the solid hard atoms assumed by Lucretius and his followers (and predecessors) to account for the permanent properties of bodies (as gold, lead, etc.) and the differences of their characters .... [A] long chain of vortex-rings, or three rings, each running through each of the others, would give each very characteristic reactions upon other such kinetic atoms.

[2]See Meleshko and Aref (2007) for a comprehensive bibliography of vortex dynamics.

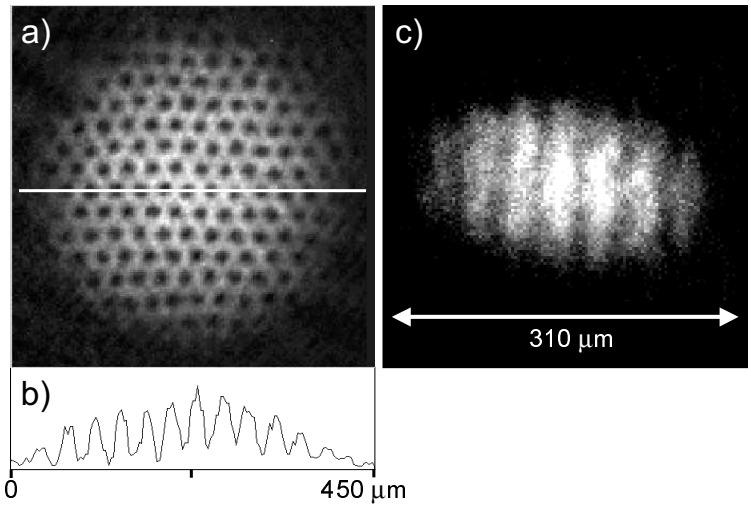

Fig. 1.4 *Front view* (a) *and horizontal cut* (b) *showing the equal spacing of the lattice sites, and side view* (c) *showing the parallel vortex filaments indicating a nearly two-dimensional structure (from Engels et al.* (2002) *(reprinted with permission from APS)).*

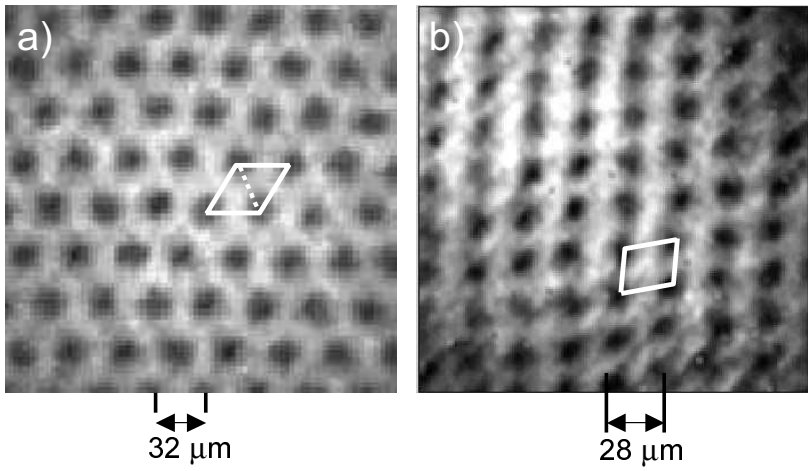

Fig. 1.5 *Under external stress, the lattice cells can change their size and shape, as shown here from Engels et al.* (2002) *(reprinted with permission from APS).*

(See Dear (2006, p. 128) for a more comprehensive discussion.) In the most optimistic scenario, a full-fledged categorization of all matter in the form of a periodic table of elements based on the links and knots of the underlying vortex rings was envisioned.[3] Shown in Figure 1.7(a) is Kelvin's symmetric arrangement of vortex rings within the

[3] A recent account of the birth and death of this "Victorian theory of everything" can be found in Kragh (2002).

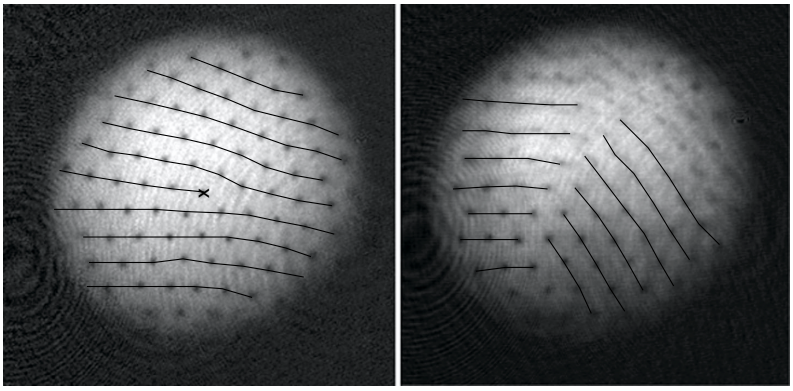

Fig. 1.6 (a) *Line defect and* (b) *grain boundary defect in the Bose–Einstein lattice, from Abo-Shaer et al.* (2001) *(reprinted with permission from AAAS).*

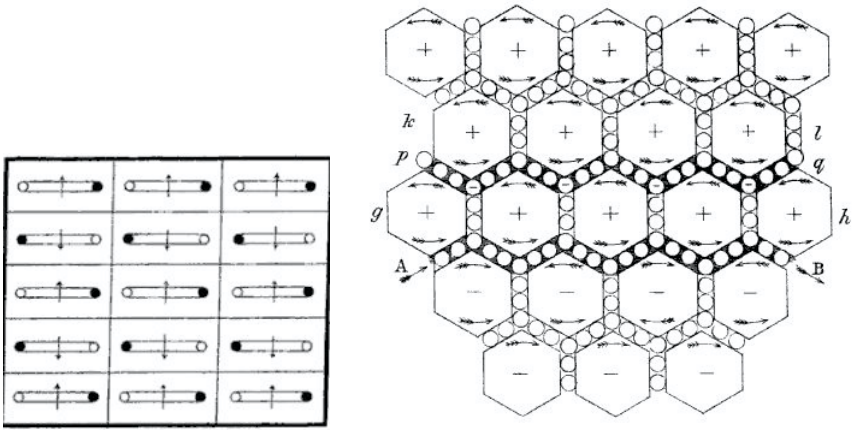

Fig. 1.7 (a) *William Thomson's (Lord Kelvin) symmetric arrangement of vortex rings (shown in cross-section) embedded in the surrounding medium as a model of the optical ether. This square lattice arrangement is made up of vortex pairs of equal and opposite sign, hence the lattice produces no net circulation and was thought to endow matter with its rigidity. Reprinted (with permission from Cambridge University Press) from Thomson* (1887). (b) *Maxwell's periodic arrangement of vortices in a lattice shown as a cross-section in the electromagnetic ether introduced the presence of what he called "idle wheel" particles between the separatrices as his mechanical model of electromagnetic phenomena. Reprinted (with permission from Dover Publications) from Maxwell* (1965).

surrounding medium, where the cross-section is made up of pairs of equal and opposite signed point vortices in a square lattice configuration with zero net circulation. In his later years he openly worried about the stability (or lack thereof) of such arrangements, and ultimately he reluctantly abandoned his grand vision of a vortex based theory of matter (see discussions in Darrigol (2005)).

In a follow-up to this "mechanistic" line of thought, Maxwell further developed Thomson's ideas and struggled with the development of what he considered a "proper

physical" treatment of electromagnetism, the purpose of which was to show that the phenomena could be made consistent with mechanical principles (Kragh (2002)). As shown in his schematic diagram in Figure 1.7(b), he represented magnetic lines by a vortex lattice, where the direction and rate of rotation of each lattice site (vortex) corresponded to the direction and strength of the magnetic field.[4] In his struggle to model what was then known about the relationship between electric currents and magnetism, he

> found great difficulty in conceiving of the existence of vortices in a medium, side by side, revolving in the same direction about parallel axes. The contiguous portions of consecutive vortices must be moving in opposite directions; and it is difficult to understand how the motion of one part of the medium can coexist with, and even produce, an opposite motion of a part in contact with it.

Maxwell's resolution was to separate the vortices by layers of particles, which he poetically called "idle wheel" particles, each revolving on its own axis in the opposite direction to that of the vortices. The idle wheel particles, when in motion, served to represent the electric current, and he used this construct of an elastic, mechanical ether to determine the amount of elasticity the medium should possess if it were indeed the cause of the electromagnetic forces measured by experiment. The model of vortices and idle wheels was, for him, a convenient fiction which allowed him to conclude that waves would travel through the medium at a speed very close to the known measured speed of light in vacuum. He thus concluded that light itself was an electromagnetic disturbance. The mechanistic model and notion of ether were, of course, ultimately discarded and are now described by historians of science as a "vehicle of intelligibility" (Dear (2006)), but the crucial insight of viewing light as an electromagnetic wave governed by Maxwell's equations is his greatest lasting contribution.

There has been a recent shift in the previous focus on *classification* of patterns, perhaps best represented by the Los Alamos catalogue of two-dimensional vortex patterns in 1978 (see Campbell and Ziff (1978, 1979) and Mertz (1978)) and the normal modes associated with linear perturbations of these patterns (see Campbell (1981), Lansky and O'Neil (1997)), toward an emphasis on the far from equilibrium *dynamics* associated with the patterns (see, for example, Engels et al. (2002)). This shift in emphasis, prompted primarily by detailed imaging and probing techniques in Bose–Einstein condensate systems, is evidenced by the beautiful visualization of "Tkachenko modes," as seen in Figure 1.8, once only a theoretical construct (Tkachenko (1966a,b), Sonin (1987)), and the formation process of highly irregular lattices (from Engels et al. (2003)), as shown in Figure 1.9. This remarkable sequence shows an initially regular lattice (frame (a)) being blasted by a laser (frame (b)), undergoing a cooling process of effectively random motion (frame (c)), before finally settling into a frozen irregular state (frame (d)). The dramatic irregularity of the state is shown in Figure 1.10 taken from Engels et al. (2002), where the histogram on top shows the regularity of the initial lattice spacings contrasted with the histogram below, showing the irregularity of the spacings. These types of experiments have exposed our lack of knowledge regarding the *formation* of the allowable patterns as well as their dynamics in the far from equilibrium regime. It has also forced us to address new questions regarding, for example, whether completely asymmetric patterns with no apparent discrete symmetries are

[4] As an interesting historical side note, one can see from the arrows in the second row from the bottom some mistakes he made in accounting for the proper circulation of each lattice site!

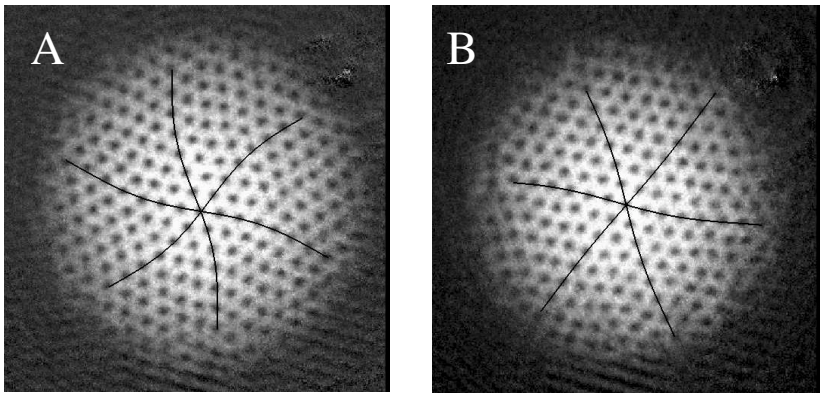

Fig. 1.8 *When perturbed by small amplitude perturbations, lattices can support linear sinusoidal waves, called "Tkachenko oscillations," shown here in a BEC lattice from Coddington et al.* (2003) *(reprinted with permission from APS).*

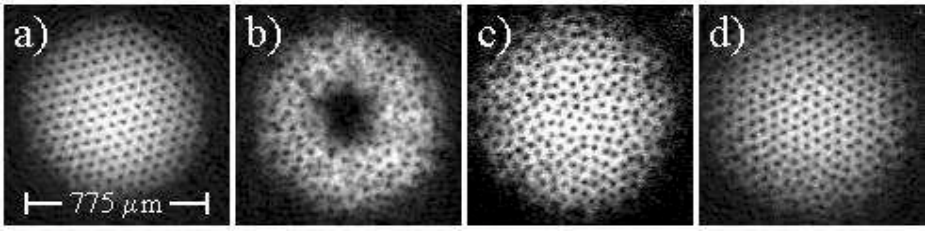

Fig. 1.9 *This sequence, published in Engels et al.* (2003) *(reprinted with permission from APS), shows an initially regular lattice (frame* (a)*) being blasted by a laser (frame* (b)*), undergoing a cooling process of seemingly random motion (frame* (c)*), before finally settling into a frozen state (frame* (d)*).*

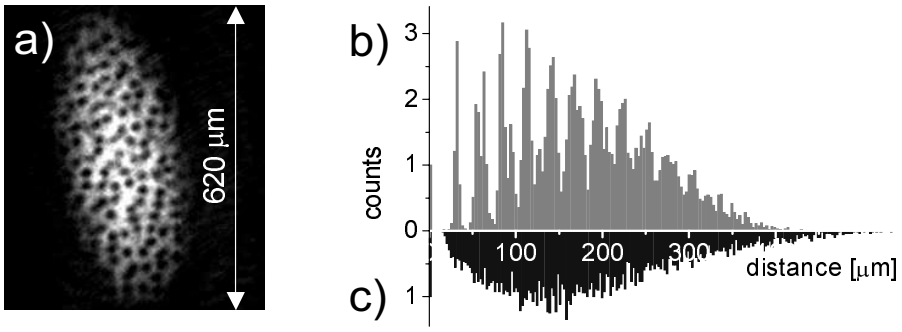

Fig. 1.10 (a) *An irregular BEC lattice from Engels et al.* (2002) *(reprinted with permission from APS). The top histogram* (b) *shows the regularity of the initial lattice spacings before the laser perturbations which destroy it, contrasted with the histogram below* (c)*, showing the final irregularity of the spacings after the "random" motion has settled.*

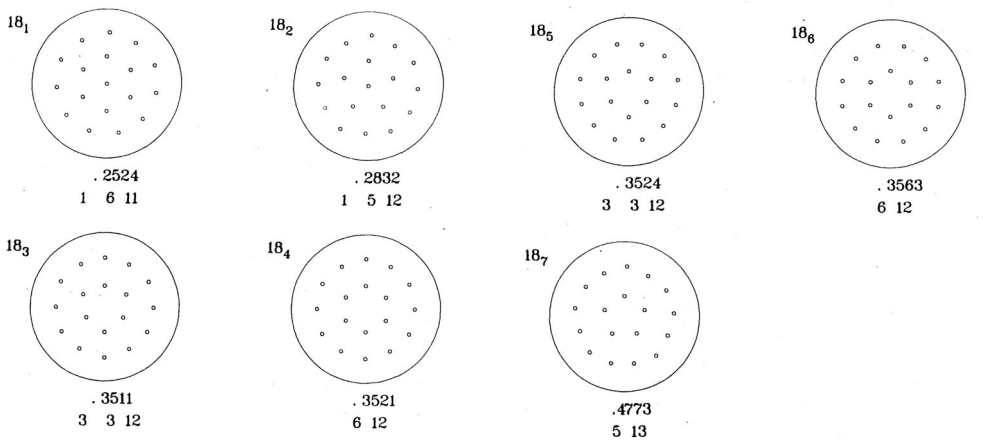

Fig. 1.11 *Panel of equal strength equilibria ($N = 18$) arranged on concentric circles taken from Campbell and Ziff* (1979) *(reprinted with permission from APS). The number just below each arrangement is the energy level, and the numbers below that show the number of vortices arranged on each of the rings, starting with the smallest. The minimum energy configuration is* (1 6 11).

allowable (see Aref and Vainchtein (1998)), and about the stability and robustness of the resulting patterns. Current questions associated with these static patterns now center on their dynamics under various forms of energetic external forcing.

Classical theory, as represented by Campbell and Ziff (1978, 1979), for example, has generally worked well at identifying allowable patterns for relatively small numbers of lattice sites (say, $N \leq 30$), sites with vortex strengths that are all equal, patterns with discernible discrete symmetries, and patterns that are stable. In these cases, the free energy landscape is not so complex, and standard techniques such as gradient search algorithms which seek out local minima, as used in Campbell and Ziff (1978, 1979), are reasonably effective. As a representative example, we show the panel of known equal strength equilibria for $N = 18$ from Campbell and Ziff (1979) in Figure 1.11. Note that, for a given value of N, there can be more than one equilibrium pattern, the energy levels that separate the patterns (number just below each pattern in the figure) can be very tightly spaced, and the number of local minima can increase rapidly (exponentially fast) with N, all of which present additional challenges.

Alternatively, when searching for patterns with known vortex strengths and identifiable discrete symmetries, an "ansatz"-based approach is a tried-and-true technique that has paid dividends (Aref (1982), Aref et al. (2003)). See Lewis and Ratiu (1996) or Aref and van Buren (2005) for two recent and representative examples of perhaps the most complex equilibrium configurations identified with this approach to date. However, for larger N (say, $N \geq 100$), heterogeneous states with unequal vortex strengths, patterns with symmetry-breaking defects or no apparent symmetries, and unstable patterns, the classical theory has not been as successful and it seems unlikely that it ever will be, since the set of allowable vortex strengths makes the energy landscape extremely high-dimensional, and their prediction is not part of the theory, but must be specified a priori.

A key aspect of the approach described in this article is that it is based on a particle-interaction point of view. In other words, since the "vorticity" at each lattice site is manifestly localized, we treat it as a "point," which implies that the

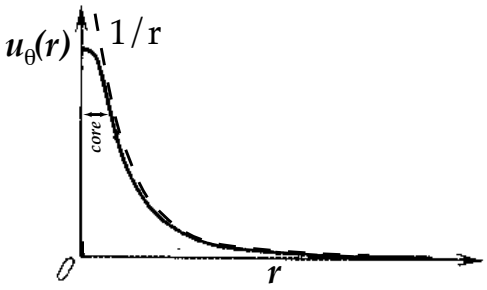

Fig. 1.12 *The solid curve shows the radial profile of the velocity field associated with an isolated lattice site; the dashed shows* $1/r$ *decay. The figure, adapted from the original version in Abrikosov's* 2003 *Nobel lecture (Abrikosov* (2004)*), is qualitative, as the axes are not marked, but shows* (i) *a vortex-core region as* $r \to 0$*, and* (ii) *monotonic decay of the field as* $r \to \infty$*.*

corresponding velocity field it generates has no azimuthal dependence, only radial. The "core size" of each vortex can be measured by the diameter, d, of each dark spot in Figure 1.3 (usually an overestimate of the core size because of fuzzy imaging) divided by a measure of the interparticle spacing, l. This dimensionless parameter $\delta = d/l \ll 1$ needs to be small in order that a particle based theory is feasible, and in most of the experiments we are referring to, $\delta \sim O(10^{-1} - 10^{-4})$. The velocity field at each site is a function whose azimuthal component, u_θ, decays monotonically with radial distance, as shown in Figure 1.12 taken from Abrikosov's Nobel lecture in 2003 (Abrikosov (2004)). Although the figure is qualitative, it exhibits two important features: (i) a core region as $r \to 0$ in which the field flattens out; (ii) monotonic decay of the field as $r \to \infty$. Since the lattice sites in our models are relatively well separated, the behavior inside the core is regarded as unimportant. The simplest way to model the monotonic decay is to use a velocity profile $u_\theta(r) = \alpha r^{-1}$, although this could be generalized to a more complicated profile if the need arose and one could also "cut off" the blow-up as $r \to 0$ in various ways (see discussions in Newton (2001)). Generally speaking, it is the monotonic decay of the radial field that is important for our purposes, not the specific profile.

Thus, we treat each site as a "particle," and the generated field is based on a linear superposition of velocity fields $\vec{u}(r) = (u_r, u_\theta) = (0, \alpha r^{-1})$ centered at each of the particle sites. The associated vorticity field ($\vec{\omega} = \nabla \times \vec{v}$) generated by this velocity is a linear superposition of delta functions, the quintessential collection of "mathematical particles." Indeed, it is in fact possible to create analog systems of interacting particles, such as large collections of millimeter-sized floating magnets on a liquid-air interface, which are capable of recreating some of the patterns seen in Bose–Einstein systems, as shown, for example, in Figure 1.13 after Grzybowski, Stone, and Whitesides (2000). For example, the patterns for the $N = 4$ and $N = 5$ states are the same as those in Figure 1.2, while the one corresponding to $N = 18$ with 6 and 11 vortices evenly spaced on two concentric circles surrounding a central vortex closely resembles the ground state shown in Figure 1.11. This work is the culmination of a long line of classical studies on pattern formation using floating magnetic devices (see, for example, Mayer (1878), Thomson (1878), Warder and Shipley (1888), Wood (1898), and Snelders (1976)). Perhaps new in this work is the focus on "dynamic" self-assembly of the magnets, each of which spins about its axis (accomplished using a

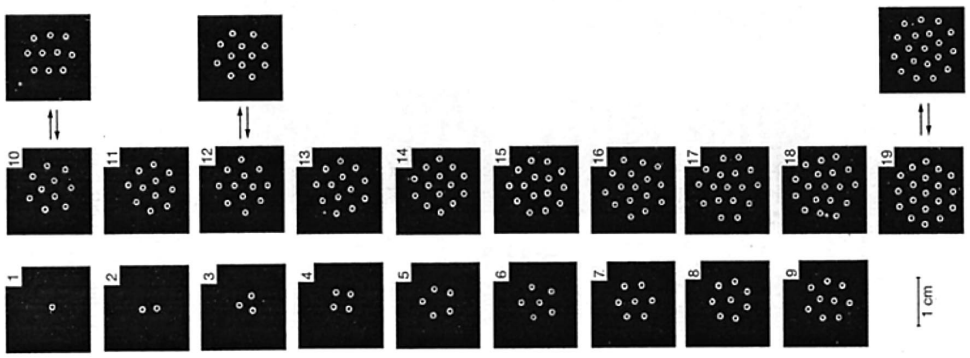

Fig. 1.13 *Dynamic self-assembly of spinning magnetic discs floating on a liquid-air interface, from Grzybowski, Stone, and Whitesides* (2000) *(reprinted with permission from Nature Publishing Group). The interaction is a combination of fluid interaction produced by the spinning discs and the magnetic field. Note that configurations for* $N = 10, 12, 19$ *are not unique and the patterns can dynamically oscillate between the two. The patterns for* $N = 4$ *and* $N = 5$ *are the same as those in Figure* 1.2. *The* $N = 18$ *pattern* $(1, 6, 11)$ *corresponds (roughly) to the lowest energy state shown in Figure* 1.11.

rotating magnet placed under the dish of liquid in which the particles float), creating an axisymmetric fluid field in the liquid about each site (in addition to the magnetic field) which decays (approximately) linearly with distance from the site. Alternatively, lattices can be produced in "random environments" using the two-dimensional Euler equations from incompressible flow, as shown in Figure 1.14, and in magnetized nonneutral plasmas (Driscoll and Fine (1990), Durkin and Fajans (2000)), as shown in Figure 1.15 (the two-dimensional Euler equations and drift-Poisson equations are isomorphic), where the vortices are magnetically confined pure electron columns. In this context, the electron density is proportional to the vorticity, while the electrostatic potential is proportional to the streamfunction, and a maximum entropy theory (see Jin and Dubin (1998)) can be used to describe the vortex crystal states, but *not* their formation or dynamics far from equilibrium.

We contrast the particle-based approach with that of treating the field as the solution of a system of partial differential equations, such as the Ginzburg–Landau or Gross–Pitaevskii equations, with highly localized (Dirac-mass) initial conditions, taking asymptotic advantage of the small parameter $\delta \equiv d/l$ in a dynamical setting. This approach has been used, for example, by Neu (1990) and was developed further by Pismen and Rubinstein (1991), Peres and Rubinstein (1993), and E (1994) and given a rigorous footing by Jerrard and Soner (1998) and Lin (1996, 1998). Two books that offer excellent state-of-the-art descriptions of much of the literature in this area are that of Bethuel, Brezis, and Helein (1994) and the most recent up-to-date account given in Sandier and Serfaty (2007), while the recent article of Zhang, Bao, and Du (2007) explores some of the same issues. Our goal in this article is to show how the particle-interaction point of view, which in a sense captures the "leading order" behavior of the asymptotic theories derived from the full nonlinear field equations, coupled with a random-walk component which mimics some of the physics and "thermodynamically" ratchets the particles toward equilibria, can be used to shed light on some questions of current research interest. For comprehensive reviews of the full equations governing Bose–Einstein and related systems, see Dalfovo et al. (1999), Leggett (2001), Aranson and Kramer (2002), and the recent article of Kevrekidis et al. (2004).

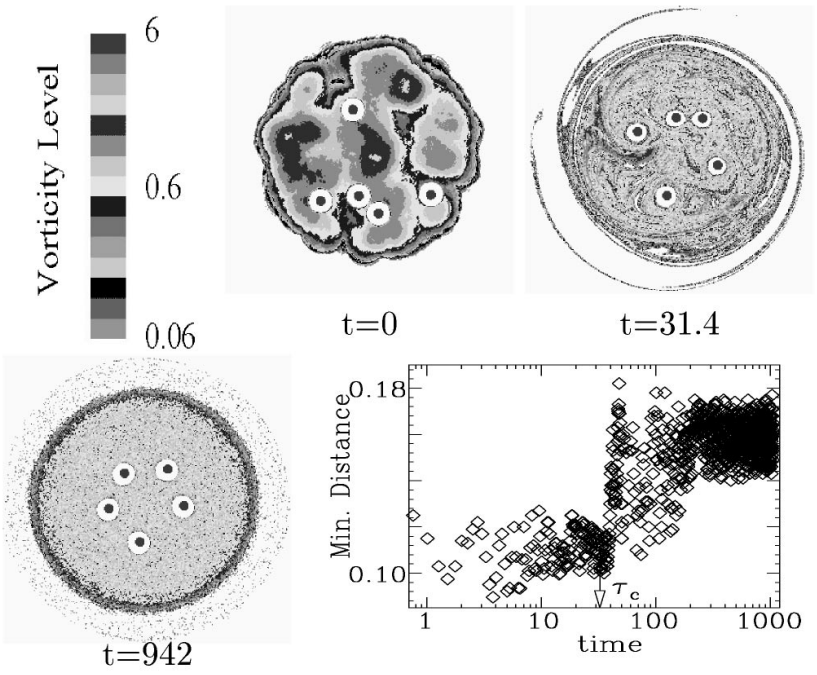

Fig. 1.14 *Lattice formation is remarkably robust, as shown here for three successive times of a vortex-in-cell simulation from Jin and Dubin* (2000) *(reprinted with permission from APS) for five point vortices in a random background. Also plotted is the minimum distance between the point vortices, with the arrow showing the approximate "cooling time" at which the crystal structure sets in.*

Fig. 1.15 *Lattices with* $N = 3, 5, 7, 9, 6$ *formed in a magnetically confined nonneutral plasma, from Fine et al.* (1995) *(reprinted with permission from APS), which mimic some of the patterns produced in Campbell and Ziff* (1978, 1979) *as well as those shown in Figures* 1.2 *and* 1.13. *The vortices are magnetically confined pure electron columns. Note that the case* $N = 9$ *appears to have a stronger vortex at the center, surrounded by* 8 *equal strength vortices around the circular perimeter.*

2. Interacting Particle Formulation. We begin with the assumption of a planar velocity field that has only radial dependence of the form $u_\theta(r) = \alpha r^{-1}$. This is most conveniently written in complex variable notation:

$$\dot{z}^* = \frac{\Gamma}{2\pi i}\frac{1}{z}, \tag{2.1}$$

where $*$ denotes complex conjugation, and $\Gamma \in \mathbb{R}$ is the particle strength, located at the origin. To see that this produces a circular field around the lattice site which decays like r^{-1} with distance, let $z(t) = r(t)\exp(i\theta(t))$, which yields

$$u_r = \dot{r} = 0, \tag{2.2}$$

$$u_\theta = r\dot{\theta} = \Gamma/2\pi r, \tag{2.3}$$

where u_r and u_θ are the radial and azimuthal velocity components, respectively. If a particle of strength $\Gamma_\beta \in \mathbb{R}$ is located at an arbitrary position $z_\beta \in \mathbb{C}$, the field produced is

$$\dot{z}^* = \frac{\Gamma_\beta}{2\pi i} \cdot \frac{1}{z - z_\beta}, \tag{2.4}$$

while the field due to a linear superposition of N of these particles is

$$\dot{z}^* = \frac{1}{2\pi i} \sum_{\beta=1}^{N} \frac{\Gamma_\beta}{z - z_\beta}. \tag{2.5}$$

Next, we make the assumption (originally due to Helmholtz) that each particle, located at position z_α ($\alpha = 1, \ldots, N$), moves according to the local velocity field, hence

$$\dot{z}_\alpha^* = \frac{1}{2\pi i} {\sum_{\beta=1}^{N}}' \frac{\Gamma_\beta}{z_\alpha - z_\beta}, \tag{2.6}$$

which is the classical dynamical system of N-point vortices (Newton (2001)). The prime on the summation indicates that the term $\beta = \alpha$ is excluded, a mathematical manifestation of the fact that a particle should have no self-induced motion and a convenient way of avoiding a singularity in the equations. Note that when all particle strengths are equal—a common but restrictive assumption—there is no loss in setting $\Gamma_\beta = 1$, since the strengths can then be pulled out of the sum and absorbed by rescaling time. Since the system is planar, we can also write it in Cartesian coordinates,

$$\vec{x}_\alpha \equiv (x_\alpha(t), y_\alpha(t)) \equiv x_\alpha + iy_\alpha = z_\alpha(t), \tag{2.7}$$

in which case we have

$$\dot{\vec{x}}_\alpha = {\sum_{\beta=1}^{N}}' \frac{\Gamma_\beta}{2\pi} \cdot \frac{\hat{n}_\beta \times (\vec{x}_\alpha - \vec{x}_\beta)}{\|\vec{x}_\alpha - \vec{x}_\beta\|^2}, \tag{2.8}$$

where

$$\hat{n}_\beta = \hat{e}_z, \tag{2.9}$$

$$l_{\alpha\beta}^2 \equiv \|\vec{x}_\alpha - \vec{x}_\beta\|^2, \tag{2.10}$$

and it is now recognizable as a "discrete Biot–Savart law" (Newton (2001)), giving the velocity field in terms of the vorticity, i.e., a discrete inversion of the linear relation $\vec{\omega} = \nabla \times \vec{v}$. It is a convenient and interesting fact that this interacting particle system is Hamiltonian,

$$\Gamma_\alpha \dot{x}_\alpha = \frac{\partial \mathcal{H}}{\partial y_\alpha}; \quad \Gamma_\alpha \dot{y}_\alpha = -\frac{\partial \mathcal{H}}{\partial x_\alpha}, \tag{2.11}$$

with $\mathcal{H}$ (originally due to Kirchhoff) given by

$$\mathcal{H} = -\frac{1}{4\pi} \sum_{\beta=1}^{N} {\sum_{\alpha=1}^{N}}' \Gamma_\alpha \Gamma_\beta \log |z_\alpha - z_\beta|. \tag{2.12}$$

In addition to $\mathcal{H}$, the other conserved quantities are the system's linear momentum and angular momentum:

$$Q + iP = \sum_{\alpha=1}^{N} \Gamma_\alpha z_\alpha, \quad I = \sum_{\alpha=1}^{N} \Gamma_\alpha |z_\alpha|^2. \tag{2.13}$$

The basis of most of the classical techniques for finding equilibria is Kelvin's variational principle (see Aref et al. (2003)), which says that equilibrium configurations arise as extremizers of the augmented Hamiltonian

$$\mathcal{H} + V \sum_{\alpha=1}^{N} \Gamma_\alpha z_\alpha + \frac{1}{2}\omega \sum_{\alpha=1}^{N} \Gamma_\alpha |z_\alpha|^2, \tag{2.14}$$

where $V = u + iv$ is the translational velocity of the configuration and ω is the rotational frequency, both of which play the role of Lagrange multipliers. See Gueron and Shafrir (1999) for an example of the use of the variational procedure in this context.

We now pose the following question in two formally different but complementary ways:

1. Given a set of N points in the complex plane with coordinates $z_\alpha(0) \in \mathbb{C}$, $\alpha = 1, \ldots, N$, find the set of vortex strengths $\vec{\Gamma} = (\Gamma_1, \Gamma_2, \ldots, \Gamma_N) \in \mathbb{R}^N$ so that all intervortical distances $l_{\alpha\beta}^2 = |z_\alpha - z_\beta|^2$ $(\alpha \neq \beta)$ remain fixed. In particular, find a basis set for this subspace of $\mathbb{R}^N$.
2. For a given set of vortex strengths $\vec{\Gamma} = (\Gamma_1, \Gamma_2, \ldots, \Gamma_N) \in \mathbb{R}^N$, find the set of points $z_\alpha(0) \in \mathbb{C}$, $\alpha = 1, \ldots, N$, so that all intervortical distances remain fixed. As a special case, there is often a reason to focus particularly on the vector of strengths $\vec{\Gamma} = (1, 1, \ldots, 1)$, as in the case of Bose–Einstein condensates, in which case all the $\Gamma_\alpha's$ in (2.6) can be absorbed by a simple rescaling of time. When N is even or infinite, another special case worthy of mention is $\vec{\Gamma} = (1, -1, 1, -1, \ldots)$, in which case they sum to zero, as in the case of a von Kármán vortex street.

We emphasize that our overriding goal for a given value of N is to find *all* configurations and all $\vec{\Gamma}$ that lead to equilibria, not just those with prespecified symmetries or assumed values of $\vec{\Gamma}$. In the next section, we describe how these questions can be addressed by understanding the nullspace structure of the "configuration" matrix associated with the lattice.

3. The Configuration Matrix. In order to derive the system governing the dynamics of the $N(N-1)/2$ intervortical distances $l_{\alpha\lambda}$, it is more convenient to start with the Cartesian formulation of the equations in the form

$$\dot{\mathbf{x}}_\alpha = {\sum_{\beta=1}^{N}}' \frac{\Gamma_\beta}{2\pi} \frac{\hat{e}_z \times (\mathbf{x}_\alpha - \mathbf{x}_\beta)}{l_{\alpha\beta}^2} \quad (\alpha = 1, \ldots, N). \tag{3.1}$$

Then

$$\begin{aligned}\dot{\mathbf{x}}_\alpha - \dot{\mathbf{x}}_\lambda &= \sum_{\beta=1}^{N}{}' \frac{\Gamma_\beta}{2\pi}\frac{\hat{e}_z \times (\mathbf{x}_\alpha - \mathbf{x}_\beta)}{l_{\alpha\beta}^2} - \sum_{\beta=1}^{N}{}' \frac{\Gamma_\beta}{2\pi}\frac{\hat{e}_z \times (\mathbf{x}_\lambda - \mathbf{x}_\beta)}{l_{\lambda\beta}^2} \\ &= \sum_{\beta=1}^{N}{}'' \frac{\Gamma_\beta}{2\pi}\frac{\hat{e}_z \times (\mathbf{x}_\alpha - \mathbf{x}_\beta)}{l_{\alpha\beta}^2} + \frac{\Gamma_\lambda}{2\pi}\frac{\hat{e}_z \times (\mathbf{x}_\alpha - \mathbf{x}_\lambda)}{l_{\alpha\lambda}^2} \\ &\quad - \sum_{\beta=1}^{N}{}'' \frac{\Gamma_\beta}{2\pi}\frac{\hat{e}_z \times (\mathbf{x}_\lambda - \mathbf{x}_\beta)}{l_{\lambda\beta}^2} - \frac{\Gamma_\alpha}{2\pi}\frac{\hat{e}_z \times (\mathbf{x}_\lambda - \mathbf{x}_\alpha)}{l_{\lambda\alpha}^2} \\ &= \sum_{\beta=1}^{N}{}'' \frac{\Gamma_\beta}{2\pi}\left[\frac{\hat{e}_z \times (\mathbf{x}_\alpha - \mathbf{x}_\beta)}{l_{\alpha\beta}^2} - \frac{\hat{e}_z \times (\mathbf{x}_\lambda - \mathbf{x}_\beta)}{l_{\lambda\beta}^2}\right] + \left(\frac{\Gamma_\alpha + \Gamma_\lambda}{2\pi}\right)\frac{\hat{e}_z \times (\mathbf{x}_\alpha - \mathbf{x}_\lambda)}{l_{\alpha\lambda}^2}.\end{aligned}$$

Using the fact that $\dot{l}_{\alpha\lambda}^2 = 2(\mathbf{x}_\alpha - \mathbf{x}_\lambda)\cdot(\dot{\mathbf{x}}_\alpha - \dot{\mathbf{x}}_\lambda)$,

$$\begin{aligned}\dot{l}_{\alpha\lambda}^2 &= 2(\mathbf{x}_\alpha - \mathbf{x}_\lambda)\cdot \sum_{\beta=1}^{N}{}'' \frac{\Gamma_\beta}{2\pi}\left[\frac{\hat{e}_z \times (\mathbf{x}_\alpha - \mathbf{x}_\beta)}{l_{\alpha\beta}^2} - \frac{\hat{e}_z \times (\mathbf{x}_\lambda - \mathbf{x}_\beta)}{l_{\lambda\beta}^2}\right] \\ &\quad + \left(\frac{\Gamma_\alpha + \Gamma_\lambda}{2\pi}\right) 2(\mathbf{x}_\alpha - \mathbf{x}_\lambda)\cdot\frac{\hat{e}_z \times (\mathbf{x}_\alpha - \mathbf{x}_\lambda)}{l_{\alpha\lambda}^2}, \\ \dot{l}_{\alpha\lambda}^2 &= \frac{1}{\pi}\sum_{\beta=1}^{N}{}''\Gamma_\beta \hat{e}_z \cdot [\mathbf{x}_\alpha \times \mathbf{x}_\beta + \mathbf{x}_\lambda \times \mathbf{x}_\alpha + \mathbf{x}_\beta \times \mathbf{x}_\lambda]\left(\frac{1}{l_{\alpha\beta}^2} - \frac{1}{l_{\lambda\beta}^2}\right).\end{aligned}$$

Noticing that $\frac{1}{2}[\mathbf{x}_\alpha \times \mathbf{x}_\beta + \mathbf{x}_\lambda \times \mathbf{x}_\alpha + \mathbf{x}_\beta \times \mathbf{x}_\lambda]$ is the area, $A_{\alpha\lambda\beta}$, subtended by the points $\mathbf{x}_\alpha$, $\mathbf{x}_\lambda$, $\mathbf{x}_\beta$, we obtain

$$\frac{d}{dt}\left(l_{\alpha\lambda}^2\right) = \frac{2}{\pi}\sum_{\beta=1}^{N}{}''\Gamma_\beta A_{\alpha\lambda\beta}\left(\frac{1}{l_{\alpha\beta}^2} - \frac{1}{l_{\lambda\beta}^2}\right) \quad (\alpha, \lambda = 1, \ldots, N). \tag{3.2}$$

Hence, the condition that all intervortical distances remain constant, $l_{\alpha\lambda}^2 = \text{const.}$, is

$$\sum_{\beta=1}^{N}{}''\Gamma_\beta A_{\alpha\lambda\beta}\left(\frac{1}{l_{\alpha\beta}^2} - \frac{1}{l_{\lambda\beta}^2}\right) = 0 \quad (\alpha, \lambda = 1, \ldots, N), \tag{3.3}$$

as long as the N particles are not collinear, in which case the subtended area collapses to zero and the configuration is degenerate (see Aref (2007b) for discussions on this point and Aref et al. (2003) for more details on the collinear states). This can be written more conveniently in matrix form:

$$A\vec{\Gamma} = 0, \tag{3.4}$$

where $A \in \mathbb{R}^{M\times N}$ has N columns and $M = N(N-1)/2$ rows and $\vec{\Gamma} = (\Gamma_1, \Gamma_2, \ldots, \Gamma_N)$. We call the matrix A the *configuration matrix* associated with the collection of N particles (not to be confused with the area term $A_{\alpha\lambda\beta}$ which, of course, appears in the entries of A), since its entries depend only on the relative positions of the particles,

not on their strengths.[5] In a sense, it encodes the *geometry* of the pattern, and not all patterns produce an equilibrium, only those corresponding to configuration matrices with nontrivial nullspaces. Existence of a lattice then depends on whether or not A has a nontrivial nullspace, giving rise to the following simple existence criterion:

$$\text{Existence:} \quad \det(A^T A) = 0. \tag{3.5}$$

The strength vector $\vec{\Gamma} \in \mathbb{R}^N$ (without loss, we can normalize it so that $\|\vec{\Gamma}\| = 1$, where $\|\cdot\|$ denotes the usual Euclidean norm in $\mathbb{R}^N$) is found a posteriori, after the pattern is set, so to speak, by finding a basis set for the nullspace of A. The strength vector is unique (with normalization condition) iff the dimension of the nullspace is one or, equivalently,

$$\text{Uniqueness:} \quad \text{Rank}(A) = N - 1. \tag{3.6}$$

Otherwise, there is more than one set of particle strengths for which that configuration is an equilibrium. Knowing the geometry of the pattern and $\vec{\Gamma}$, we can find the translational velocity V, the rotational frequency ω, and the Hamiltonian energy (2.12) of the lattice, whose equations are derived in Aref et al. (2003). In fact, in some cases, particularly elegant and useful formulas for the Hamiltonian energy can be obtained (see Gueron and Shafrir (1999) and Aref (2007c)). In the remainder of the article, we will focus on the structure of the configuration matrix A instead of the actual configuration of N particles, as specified by their positions in the complex plane.

3.1. The Triangle. Consider a general triangle shown in Figure 3.1(a). The configuration matrix formed from (3.3) is

$$A = \begin{pmatrix} A_{231}\left(\frac{1}{l_{21}^2} - \frac{1}{l_{31}^2}\right) & 0 & 0 \\ 0 & A_{312}\left(\frac{1}{l_{32}^2} - \frac{1}{l_{12}^2}\right) & 0 \\ 0 & 0 & A_{123}\left(\frac{1}{l_{13}^2} - \frac{1}{l_{23}^2}\right) \end{pmatrix}. \tag{3.7}$$

With only three particles, the areas are all equal and we write $A_{ijk} \equiv \Delta$, which we factor out of the matrix leaving a simple matrix with diagonal structure,

$$A = \Delta \begin{pmatrix} a_1 & 0 & 0 \\ 0 & a_2 & 0 \\ 0 & 0 & a_3 \end{pmatrix}, \tag{3.8}$$

where $a_1 = (\frac{1}{l_{21}^2} - \frac{1}{l_{31}^2})$, $a_2 = (\frac{1}{l_{12}^2} - \frac{1}{l_{32}^2})$, $a_3 = (\frac{1}{l_{13}^2} - \frac{1}{l_{23}^2})$. If none of the sides is equal to another, $a_1 \neq a_2 \neq a_3$, there are no zero eigenvalues, the rank is three, and

[5] The configuration matrices discussed in this article are based on collections of particles in the unbounded plane, which one can think of as analogous to constructing a lattice in an isotropic medium. To carry the analogy further, if one wanted to ask how the crystalline structure of the material imposes itself on the allowable lattice patterns (to satisfy Landau's curiosity), one could work in domains enclosed by solid boundaries; in this case an additional (at least) N "image" particles, of appropriate strengths (for lattice cells with appropriate symmetries), would be placed outside the domain, at fixed distances from their "preimages" inside the domain, in order to enforce the condition that the boundary be a streamline. One would still construct the configuration matrix based only on the N particles inside the domain, hence its size would be the same as if the boundary were absent.

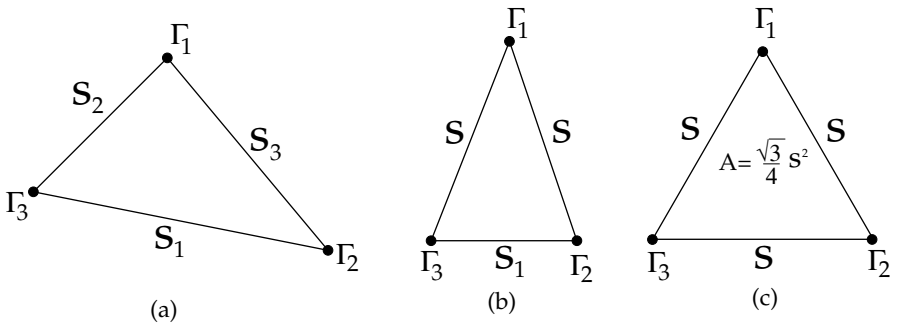

Fig. 3.1 *$N = 3$: Triangular lattice cell:* (a) *General triangle;* (b) *isosceles triangle;* (c) *equilateral with side s and area $A = \sqrt{3}s^2/4$.*

the nullspace is empty, allowing us to conclude that there are no nontrivial particle strengths $\vec{\Gamma}$ for which an equilibrium exists. If the triangle is isosceles with two sides equal (Figure 3.1(b)), say, $l_{12} = l_{13} \neq l_{23}$, then $a_1 = 0$, $a_2 \neq 0$, and $a_3 \neq 0$, the matrix has a single eigenvalue which is zero, the rank is two, and the nullspace is one-dimensional with basis $(1, 0, 0)^T$, i.e., the particle opposite the unequal side can have any value, while the other two must have value zero. This corresponds to the trivial case of one vortex Γ_1 with two passive particles rotating in the same circular orbit around it—certainly an equilibrium but not a very interesting one! Finally, if the triangle is equilateral (Figure 3.1(c)), then $a_1 = a_2 = a_3 = 0$, the rank is zero, and the nullspace is three-dimensional with basis set $\{(1, 0, 0)^T, (0, 1, 0)^T, (0, 0, 1)^T\}$. The three vortex strengths can be chosen to have any value independently and the equilateral triangle will always be an equilibrium. This configuration, with $\Gamma_1 = \Gamma_2 = \Gamma_3$, is the one shown in Figure 1.2(c) in superfluid helium, Figure 1.13(3) with collections of spinning magnets, and Figure 1.15(a) in a magnetically confined nonneutral plasma. The method also shows how the extreme symmetry of the equilateral triangle is the reason it is an equilibrium, for if any of the three positions is slightly perturbed, the matrix will again have full rank and empty nullspace. Furthermore, if we place a fourth particle at random in the plane, as shown in Figure 3.2, its distance from each of the other three will be distinct, and the configuration matrix associated with the four points will generically have a zero-dimensional nullspace. This is despite the fact that the configuration is known to be linearly stable (Havelock (1931)). One can find formulas for the rotational frequencies and translational velocities associated with the equilateral triangle in Aref et al. (2003). One might say, from this example, that a stable configuration is *not* necessarily a robust one.

3.2. The Singular Value Decomposition of the Configuration Matrix. For larger N, a more systematic procedure is needed. The most comprehensive tool for understanding and characterizing the nullspace, range, and rank of any matrix is the singular value decomposition (SVD; see Golub and Van Loan (1996)). It is a factorization that greatly generalizes the spectral decomposition of a matrix, as the SVD is available for any matrix. For our purposes, since $A \in \mathbb{R}^{M \times N}$, we formulate the SVD for real matrices only, although the generalization to the complex case is standard (see Golub and Van Loan (1996) or Trefethen and Bau (1997)). The N singular values, $\sigma^{(i)}$ $(i = 1, \ldots, N)$, of the M by N real matrix A are nonnegative real

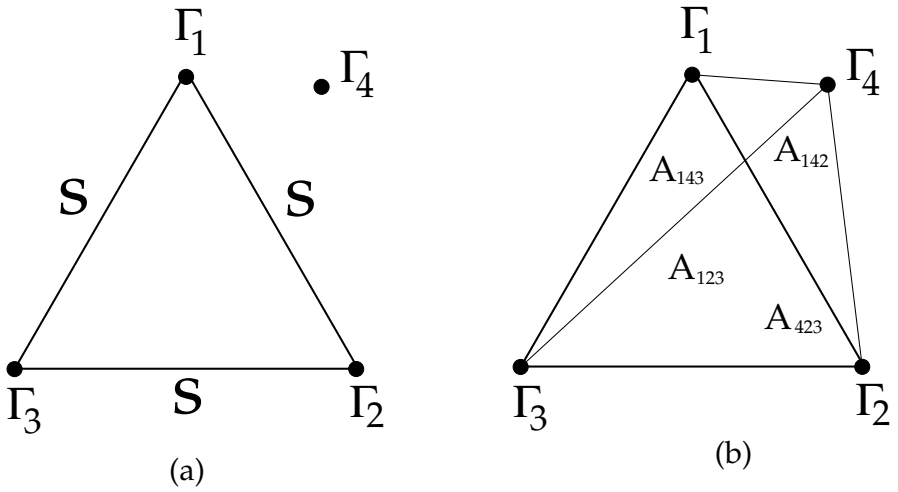

Fig. 3.2 (a) *Equilateral triangle with a fourth particle deposited randomly.* (b) *Symmetry is destroyed, which changes the matrix from one with a nullspace dimension of three to one with a zero-dimensional nullspace, hence full rank. The equilateral triangle is dynamically stable (Havelock* (1931)*), but its configuration matrix is not robust.*

numbers that satisfy

$$A\mathbf{v}^{(i)} = \sigma^{(i)}\mathbf{u}^{(i)}; \quad A^T\mathbf{u}^{(i)} = \sigma^{(i)}\mathbf{v}^{(i)}, \tag{3.9}$$

where $\mathbf{u}^{(i)} \in \mathbb{R}^M$ and $\mathbf{v}^{(i)} \in \mathbb{R}^N$. The vector $\mathbf{u}^{(i)}$ is called the left-singular vector associated with $\sigma^{(i)}$, while $\mathbf{v}^{(i)}$ is the right-singular vector. In terms of these vectors, the matrix A has the factorization

$$A = U\Sigma V^T. \tag{3.10}$$

Since $M > N$, the first N columns of U are the left-singular vectors $\mathbf{u}^{(i)}$, and the remaining $M - N$ columns are chosen to be orthonormal so that U is orthogonal ($U^TU = I$). Then U is an $M \times M$ orthogonal matrix, V is an $N \times N$ orthogonal matrix whose columns are the right-singular vectors $\mathbf{v}^{(i)}$, and Σ is an $M \times N$ matrix with the N singular values on the diagonal and zeros off the diagonal:

$$\Sigma = \begin{pmatrix} \sigma^{(1)} & \cdots & 0 \\ & \ddots & \\ 0 & \cdots & \sigma^{(N)} \\ 0 & \cdots & 0 \\ \vdots & & \vdots \\ 0 & \cdots & 0 \end{pmatrix}. \tag{3.11}$$

The singular values can be ordered so that $\sigma^{(1)} \equiv \sigma^{(\max)} \geq \sigma^{(2)} \geq \cdots \geq \sigma^{(\min)} \geq 0$ and one or more may be zero. As is evident from multiplying the first equation in (3.9) by A^T and the second by A,

$$(A^TA - \sigma^{(i)2})\mathbf{v}^{(i)} = 0, \quad (AA^T - \sigma^{(i)2})\mathbf{u}^{(i)} = 0, \tag{3.12}$$

the singular values squared are the eigenvalues of the *covariance* matrices A^TA or AA^T, which have the same eigenvalue structure, while the left-singular vectors $\mathbf{u}^{(i)}$ are the eigenvectors of AA^T and the right-singular vectors $\mathbf{v}^{(i)}$ are the eigenvectors of A^TA. From (3.9), we also note that the right-singular vectors $\mathbf{v}^{(i)}$ corresponding to $\sigma^{(i)} = 0$ form a basis for the nullspace of A.[6]

We seek configuration matrices with one or more singular values that are zero, and the SVD provides an explicit and optimal representation of the range and nullspace of the matrix A. In particular, the right-singular vectors $\mathbf{v}^{(i)}$ corresponding to the singular values that are zero span the nullspace of A, while the left-singular vectors $\mathbf{u}^{(i)}$ corresponding to the nonzero singular values span the range of A. The rank of A equals the number of nonzero singular values and, since $\text{rank}(A) + \text{nullity}(A) = N$, we know that the number of zero singular values equals the dimension of the nullspace of A. Also, the ranks of A, A^TA, AA^T are the same and A^TA and AA^T have the same nonzero eigenvalues and nullspaces.

The formula (3.9), which defines the singular values, also lends itself nicely to a "Rayleigh quotient" interpretation. If we write the first equation (dropping superscripts) as

$$\sigma\mathbf{u} = A\mathbf{v}, \tag{3.13}$$

and think of $\mathbf{u}$ as the unknown in a least-squares formulation, then the associated normal equations obtained by multiplying each side by $\mathbf{u}^T$ gives rise to the best approximate solution

$$\sigma\mathbf{u}^T\mathbf{u} = \mathbf{u}^TA\mathbf{v}, \tag{3.14}$$

or

$$\sigma = \frac{\mathbf{u}^TA\mathbf{v}}{\mathbf{u}^T\mathbf{u}} = \mathbf{u}^TA\mathbf{v}, \tag{3.15}$$

for vectors of unit length. Thus, for arbitrary unit vectors $\mathbf{u}, \mathbf{v}$, the scalar σ that acts most like a singular value of A is the one shown above, as it minimizes the residual $\|\sigma\mathbf{u} - A\mathbf{v}\|_2$.[7] If in fact the vectors $\mathbf{u}, \mathbf{v}$ are the left- and right-singular vectors of A, then the residual is zero and σ is exactly the singular value.

3.3. The Square. A good example which shows the utility of the SVD is the square configuration shown in Figure 3.3(a), which also can be thought of as four vortices equally spaced on the circumference of a circle, one of the classical configurations treated in Havelock (1931), which is known to be linearly stable. The configuration

[6] It is interesting to point out that many of the properties of the SVD were discussed and proven in a very direct way by Keller (1962), who knew and built upon Hotelling's 1933 treatment of the principal component analysis in statistics.

[7] Here $\|\cdot\|_2$ denotes the 2-norm.

matrix has banded structure:

(3.16)
$$A = \begin{pmatrix} A_{341}\left(\frac{1}{l_{31}^2}-\frac{1}{l_{41}^2}\right) & A_{342}\left(\frac{1}{l_{32}^2}-\frac{1}{l_{42}^2}\right) & 0 & 0 \\ A_{241}\left(\frac{1}{l_{21}^2}-\frac{1}{l_{41}^2}\right) & 0 & A_{243}\left(\frac{1}{l_{23}^2}-\frac{1}{l_{43}^2}\right) & 0 \\ A_{231}\left(\frac{1}{l_{21}^2}-\frac{1}{l_{31}^2}\right) & 0 & 0 & A_{234}\left(\frac{1}{l_{24}^2}-\frac{1}{l_{34}^2}\right) \\ 0 & A_{142}\left(\frac{1}{l_{12}^2}-\frac{1}{l_{42}^2}\right) & A_{143}\left(\frac{1}{l_{13}^2}-\frac{1}{l_{43}^2}\right) & 0 \\ 0 & A_{132}\left(\frac{1}{l_{12}^2}-\frac{1}{l_{32}^2}\right) & 0 & A_{134}\left(\frac{1}{l_{14}^2}-\frac{1}{l_{34}^2}\right) \\ 0 & 0 & A_{123}\left(\frac{1}{l_{13}^2}-\frac{1}{l_{23}^2}\right) & A_{124}\left(\frac{1}{l_{14}^2}-\frac{1}{l_{24}^2}\right) \end{pmatrix}$$

(3.17)
$$= \left(\frac{d^2-s^2}{2d^2}\right)\Delta \begin{pmatrix} 1 & -1 & 0 & 0 \\ 0 & 0 & 0 & 0 \\ -1 & 0 & 0 & 1 \\ 0 & 1 & -1 & 0 \\ 0 & 0 & 0 & 0 \\ 0 & 0 & 1 & -1 \end{pmatrix} = \frac{1}{4}\begin{pmatrix} 1 & -1 & 0 & 0 \\ 0 & 0 & 0 & 0 \\ -1 & 0 & 0 & 1 \\ 0 & 1 & -1 & 0 \\ 0 & 0 & 0 & 0 \\ 0 & 0 & 1 & -1 \end{pmatrix},$$

where $\Delta \equiv s^2/2$ is the area subtended by any three particles and $d^2 = 2s^2$. The SVD of A gives rise to the matrices

(3.18)
$$U = \begin{pmatrix} -0.5 & 0.5 & 0.5 & -0.1015 & 0 & 0.4896 \\ 0 & 0 & 0 & 0.9792 & 0 & 0.2030 \\ 0.5 & -0.5 & 0.5 & -0.1015 & 0 & 0.4896 \\ 0.5 & 0.5 & -0.5 & -0.1015 & 0 & 0.4896 \\ 0 & 0 & 0 & 0 & 1.0 & 0 \\ -0.5 & -0.5 & -0.5 & -0.1015 & 0 & 0.4896 \end{pmatrix},$$

(3.19)
$$\Sigma = \begin{pmatrix} \frac{1}{2} & 0 & 0 & 0 \\ 0 & \frac{1}{2\sqrt{2}} & 0 & 0 \\ 0 & 0 & \frac{1}{2\sqrt{2}} & 0 \\ 0 & 0 & 0 & 0 \\ 0 & 0 & 0 & 0 \\ 0 & 0 & 0 & 0 \end{pmatrix},$$

(3.20)
$$V = \begin{pmatrix} -0.5 & 0.7071 & 0 & -0.5 \\ 0.5 & 0 & -0.7071 & -0.5 \\ -0.5 & -0.7071 & 0 & -0.5 \\ 0.5 & 0 & 0.7071 & -0.5 \end{pmatrix}.$$

Hence, the singular values are $(\sigma^{(1)}, \sigma^{(2)}, \sigma^{(3)}, \sigma^{(4)}) = (\frac{1}{2}, \frac{1}{2\sqrt{2}}, \frac{1}{2\sqrt{2}}, 0)$, giving rise to a one-dimensional nullspace with basis $(-0.5, -0.5, -0.5, -0.5)$ (the rightmost column of V), i.e., the four vortices must have equal strength. This is precisely the superfluid helium configuration shown in Figure 1.2(d) and the spinning magnet configuration in Figure 1.13(4).

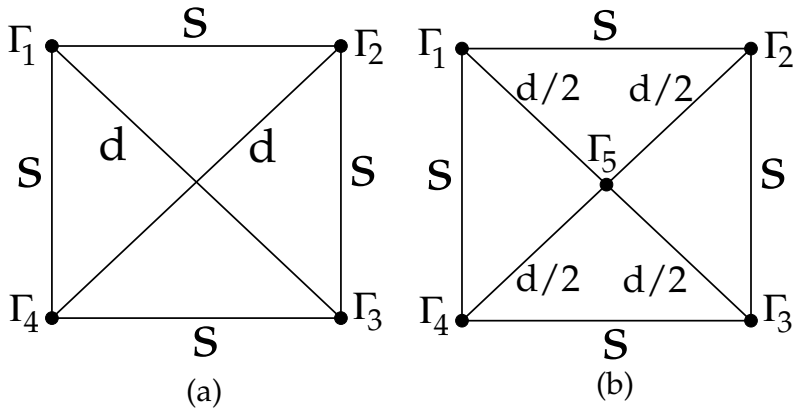

Fig. 3.3 (a) *Square lattice cell with side s. The (normalized) singular values are* $(\frac{1}{2}, \frac{1}{4}, \frac{1}{4}, 0)$ *with Shannon entropy* $\frac{3}{2}\ln(2) = 1.0397$. (b) *Square lattice cell with side s and a central vortex. The (normalized) singular values are* $(\frac{3}{8}, \frac{3}{8}, \frac{1}{4}, 0, 0)$ *with Shannon entropy* $\frac{7}{4}\ln(2) - \frac{3}{4}\ln(3) = 0.3890$. *See text for details.*

With an additional vortex at the center, as shown in Figure 3.3(b), one can show that the configuration matrix is

$$A = \frac{1}{4}\begin{pmatrix} -1 & 0 & 1 & 0 & 0 \\ 0 & 1 & 0 & -1 & 0 \\ 1 & -1 & 0 & 0 & 0 \\ 1 & 0 & -1 & 0 & 0 \\ 0 & 0 & 0 & 0 & 0 \\ -1 & 0 & 0 & 1 & 0 \\ 0 & -1 & 0 & 1 & 0 \\ 0 & 1 & -1 & 0 & 0 \\ 0 & 0 & 0 & 0 & 0 \\ 0 & 0 & 1 & -1 & 0 \end{pmatrix}. \tag{3.21}$$

The SVD of A gives rise to the matrices

$$U = \begin{pmatrix} -0.5774 & 0 & 0 & -0.2224 & 0 & -0.4104 & -0.4554 & 0.4242 & 0 & -0.2480 \\ 0 & 0.5774 & 0 & -0.7195 & 0 & 0.1906 & 0.1621 & -0.1622 & 0 & -0.2452 \\ 0.2887 & -0.2887 & -0.5 & -0.0908 & 0 & 0.4348 & -0.0615 & 0.4559 & 0 & -0.4176 \\ 0.5774 & 0 & 0 & -0.2993 & 0 & -0.1692 & -0.6566 & -0.0410 & 0 & 0.3399 \\ 0 & 0 & 0 & 0 & 1 & 0 & 0 & 0 & 0 & 0 \\ -0.2887 & -0.2887 & 0.5 & -0.1677 & 0 & 0.6760 & -0.2628 & -0.0093 & 0 & 0.1703 \\ 0 & -0.5774 & 0 & -0.5481 & 0 & -0.2729 & 0.4556 & 0.0975 & 0 & 0.2733 \\ 0.2887 & 0.2887 & 0.5 & 0.0806 & 0 & -0.0286 & 0.2320 & 0.7155 & 0 & 0.1009 \\ 0 & 0 & 0 & 0 & 0 & 0 & 0 & 0 & 1.0 & 0 \\ -0.2887 & 0.2887 & -0.5 & 0.0037 & 0 & 0.2126 & 0.0307 & 0.2504 & 0 & 0.6888 \end{pmatrix}, \tag{3.22}$$

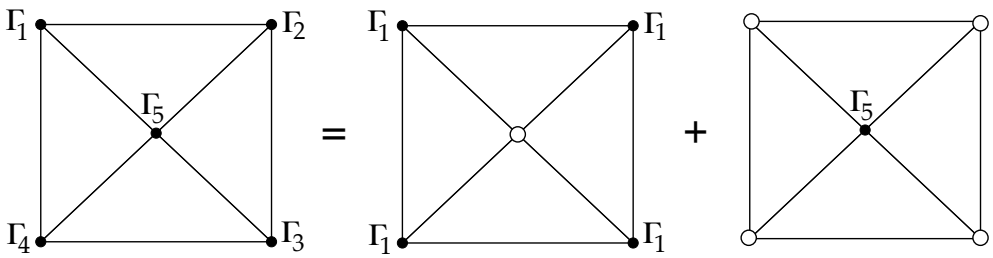

Fig. 3.4 *The decomposition of the square with a center vortex into its optimal basis elements via the SVD of its configuration matrix. Open circles are passive particles, or vortices of zero strength.*

$$\Sigma = \begin{pmatrix} \frac{\sqrt{3}}{2\sqrt{2}} & 0 & 0 & 0 & 0 \\ 0 & \frac{\sqrt{3}}{2\sqrt{2}} & 0 & 0 & 0 \\ 0 & 0 & 1/2 & 0 & 0 \\ 0 & 0 & 0 & 0 & 0 \\ 0 & 0 & 0 & 0 & 0 \\ 0 & 0 & 0 & 0 & 0 \\ 0 & 0 & 0 & 0 & 0 \\ 0 & 0 & 0 & 0 & 0 \\ 0 & 0 & 0 & 0 & 0 \\ 0 & 0 & 0 & 0 & 0 \end{pmatrix}, \tag{3.23}$$

$$V = \begin{pmatrix} 0.7071 & 0 & -0.5 & 0.5 & 0 \\ 0 & 0.7071 & 0.5 & 0.5 & 0 \\ -0.7071 & 0 & -0.5 & 0.5 & 0 \\ 0 & -0.7071 & 0.5 & 0.5 & 0 \\ 0 & 0 & 0 & 0 & 1 \end{pmatrix}. \tag{3.24}$$

The singular values in this case are $(\sigma^{(1)}, \sigma^{(2)}, \sigma^{(3)}, \sigma^{(4)}, \sigma^{(5)}) = (\frac{\sqrt{3}}{2\sqrt{2}}, \frac{\sqrt{3}}{2\sqrt{2}}, \frac{1}{2}, 0, 0)$, and the nullspace is two-dimensional with basis set $\{(0.5, 0.5, 0.5, 0.5, 0)^T, (0, 0, 0, 0, 1)^T\}$ (the two rightmost columns of V), indicating that any linear combination of a central vortex with equal strength vortices on the four corners will form an equilibrium, as shown in Figure 3.4. Notice also that the method tells us that the four equal strength vortices produce a stagnation point at the center, an extra piece of important information as stagnation points are known to be crucial in studying aspects of mixing and transport of passive particles in the flowfield (see, for example, Aref and Brøns (1998)), a topic we comment on at the end of the article.

3.4. What Do the Other Singular Values Tell Us? The configuration matrix A contains a wealth of geometric information about the lattice which is encoded in the full set of singular values. First, if we normalize each of the eigenvalues of the covariance matrix $A^T A$ by dividing by their sum,

$$\hat{\lambda}_i = \frac{\lambda_i}{\sum_{j=1}^{N} \lambda_j} \quad (i = 1, \ldots, N) \tag{3.25}$$

(recall that $(\sigma^{(i)})^2 \equiv \lambda_i$), then each can be interpreted as the *probability* $P_i \equiv \hat{\lambda}_i$ that the pattern will be clustered in that mode (singular vector). It can also be interpreted

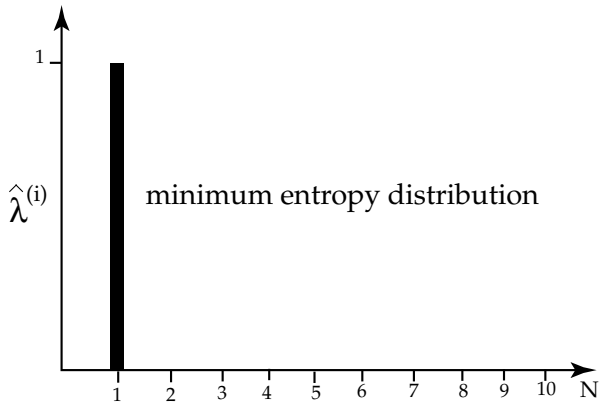

Fig. 3.5 *Singular value distribution corresponding to a matrix of minimum entropy. All of the energy is clustered into one mode.*

as the fraction of the total energy residing in that mode. The discrete sequence $(P_1, P_2, \ldots, P_N)$ then contains important information about the way in which the lattice is structured. From this, we can define a scalar measure of information content, or Shannon entropy (see Shannon (1948)), H, of the pattern

$$H = -\sum_{i=1}^{N} P_i \ln P_i. \tag{3.26}$$

To see the utility of this quantity, it is useful to compare two extreme examples—one with minimal entropy and one with maximal entropy (see Kirby (2001)).

Example 1. Consider the case where $P_1 = 1$, $P_i = 0$ for $i > 1$, i.e., all the energy is clustered in one mode. In this case, $H = 0$, which is minimum, and information compression is maximal. The simplest example of a minimum entropy matrix is the square $N \times N$ matrix

$$A = \begin{pmatrix} 1 & 0 & \ldots & 0 & 0 \\ 0 & 0 & \ldots & 0 & 0 \\ 0 & 0 & \ldots & 0 & 0 \\ \vdots & \vdots & \ddots & \vdots & \vdots \\ 0 & 0 & \ldots & 0 & 0 \end{pmatrix}. \tag{3.27}$$

For this matrix, $A^T A = A$, which has rank one and nullspace dimension $N-1$. There is one nonzero singular value, while the other $N-1$ are zero. This case is depicted in Figure 3.5.

Example 2. Consider the case where all probabilities are equal, hence $P_i = \frac{1}{N}$, for $i = 1, \ldots, N$. In this case, $H = \ln N$, which is maximum. There is no information compression or preferred coordinate clustering in this case. Every orthogonal matrix ($A^T = A^{-1}$) is a maximum entropy matrix, since $A^T A = AA^T = I$, which implies $\lambda_i = 1$, $\hat{\lambda}_i = 1/N$ $(i = 1, \ldots, N)$. The simplest example is the identity matrix, whose covariance matrix is also the identity matrix, with unit eigenvalues and uniform distribution among the singular modes. This case is depicted in Figure 3.6.

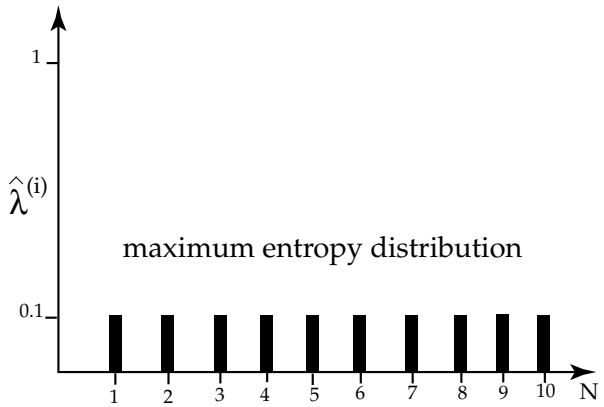

Fig. 3.6 *Singular value distribution corresponding to a matrix of maximum entropy. The energy is spread evenly across all modes.*

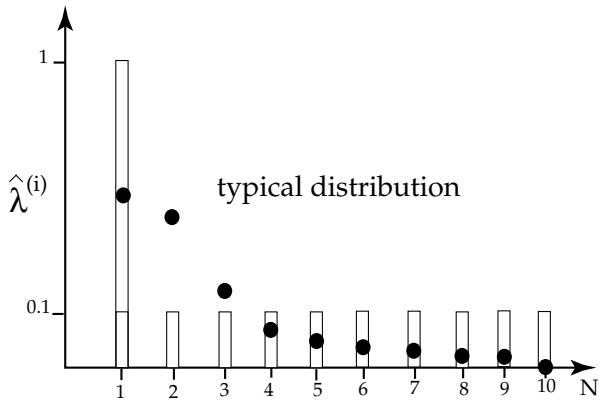

Fig. 3.7 *A typical distribution of singular values, as compared with the minimum and maximum distributions. The singular values are ordered from largest to smallest, with the last one being zero, indicating that the lattice of ten vortices has a one-dimensional nullspace with unique values for the vortex strengths. Lower entropy lattices have configuration matrices that are closer to matrices of low rank.*

The typical singular value distribution for a lattice, as compared with these two extremes, is shown in Figure 3.7. One can state that distributions of singular values that drop off sharply from the maximum (Example 1) are *lower* entropy matrices then those that are relatively flat around the maximum (Example 2). Stated differently, the percentage of information compression can be measured from the quantity

$$\left(\frac{\ln N - H}{\ln N}\right) \cdot 100, \tag{3.28}$$

which in the first example gives 0%, while in the second gives 100%. In Shannon's original paper (1948), he makes an interesting observation about the quantity (3.26). He proves that *any change toward equalization of probabilities* $P_1, P_2, \ldots, P_n$ *will increase* H. In particular, if we perform any operation on these probabilities which

"averages" them, i.e., let

$$P_i' = \sum_j a_{ij} P_j, \tag{3.29}$$

where $\sum_i a_{ij} = \sum_j a_{ij} = 1$ with $a_{ij} \geq 0$, then H increases. Since generic perturbations of the configuration matrix A will generally spread the P_i's more evenly, this will increase H. It follows that configurations with larger values of H will change less under perturbation than those with smaller values of H, and in this sense we say that they are more *robust*.

For the square configuration with no central vortex, $N = 4$, the normalized eigenvalues are given by

$$(\hat{\lambda}_1, \hat{\lambda}_2, \hat{\lambda}_3, \hat{\lambda}_4) = (P_1, P_2, P_3, P_4) = \left(\frac{1}{2}, \frac{1}{4}, \frac{1}{4}, 0\right), \tag{3.30}$$

hence the entropy is given by

$$\begin{aligned} H &= -\sum_{i=1}^{4} P_i \ln P_i = -\frac{1}{2}\ln(1/2) - \frac{1}{4}\ln(1/4) - \frac{1}{4}\ln(1/4) \\ &= \frac{1}{2}\ln 2 + \frac{1}{2}\ln 4 = \frac{3}{2}\ln 2 = 1.0397. \end{aligned} \tag{3.31}$$

The maximum entropy for $N = 4$ is $\ln 4 = 1.3863$, hence the percentage of information compression as measured by (3.28) is 25%. For the square configuration with a central vortex, $N = 5$, the normalized eigenvalues are

$$(\hat{\lambda}_1, \hat{\lambda}_2, \hat{\lambda}_3, \hat{\lambda}_4, \hat{\lambda}_5) = (P_1, P_2, P_3, P_4, P_5) = \left(\frac{3}{8}, \frac{3}{8}, \frac{1}{4}, 0, 0\right), \tag{3.32}$$

hence the entropy is given by

$$\begin{aligned} H &= -\sum_{i=1}^{4} P_i \ln P_i = -\frac{3}{8}\ln(3/8) - \frac{3}{8}\ln(3/8) - \frac{1}{4}\ln(1/4) \\ &= -\frac{3}{4}\ln 3 + \frac{7}{4}\ln 2 = 0.3890. \end{aligned} \tag{3.33}$$

The maximum entropy for $N = 5$ is $\ln 5 = 1.6094$, hence the percentage of information compression as measured by (3.28) is 76%. Our conclusion is that the square *without* a central vortex is a higher entropy state than one *with* a central vortex, i.e., there is a more even distribution of energy among the modes and the configuration is more robust. In addition, there is less compression of information with respect to the idealized state of maximum entropy. It is perhaps relevant to point out that for $N = 4$, the square configuration also has higher entropy than the equilateral triangle with an additional vortex at the center. Likewise, for $N = 5$, the regular pentagon has higher entropy than the square with a fifth vortex placed at the center. In both these cases, it is the regular configuration *without* the vortex at the center that appears in experiments such as those in Figures 1.2 and 1.13. Both are lower energy states (see Gueron and Shafrir (1999)) and higher entropy states than the corresponding ones with the central vortex (for the same value of N).

The second important piece of geometric information buried in the full set of singular values is the *size* of the lattice, as measured by the Frobenius norm $\|A\|_F$ of the configuration matrix or, alternatively, the 2-norm $\|A\|_2$:

$$\|A\|_2 = \sigma^{(1)} \leq \|A\|_F^2 = (\sigma^{(1)})^2 + \cdots + (\sigma^{(r)})^2 \equiv \text{trace}(A^T A). \tag{3.34}$$

Both of these norms are useful since they are invariant under multiplication by unitary matrices (Trefethen and Bau (1997)), hence they can be written directly in terms of the singular values down the diagonal of Σ (since the matrices U and V are orthogonal). For the square lattice without the central vortex, the lattice size is given by

$$\begin{aligned} \|A\|_F^2 &= \left(\frac{1}{2}\right)^2 + \left(\frac{1}{2\sqrt{2}}\right)^2 + \left(\frac{1}{2\sqrt{2}}\right)^2 = \frac{1}{2}, \\ \|A\|_2 &= \frac{1}{2}. \end{aligned} \tag{3.35}$$

With the central vortex, the lattice is larger since in this case

$$\begin{aligned} \|A\|_F^2 &= \left(\frac{\sqrt{3}}{2\sqrt{2}}\right)^2 + \left(\frac{\sqrt{3}}{2\sqrt{2}}\right)^2 + \left(\frac{1}{2}\right)^2 = 1, \\ \|A\|_2 &= \frac{\sqrt{3}}{2\sqrt{2}}. \end{aligned} \tag{3.36}$$

In addition, knowing the full set of singular values for two different configurations with the same number of particles allows us to compare their entropies by computing their *Kullback–Leibler divergence* (also called *relative entropy*), a standard way of comparing two different distributions (Kullback and Leibler (1951)). This value is defined as

$$D_{KL}(P,Q) = \sum_{i=1}^{N} P_i \ln \frac{P_i}{Q_i}, \tag{3.37}$$

where $P = (P_1, P_2, \ldots, P_N)$ and $Q = (Q_1, Q_2, \ldots, Q_N)$ are the two distributions being compared. It can be understood by noting that

$$\begin{aligned} D_{KL}(P,Q) &= \sum_{i=1}^{N} P_i \ln(P_i) - \sum_{i=1}^{N} P_i \ln(Q_i) \\ &= -\sum_{i=1}^{N} P_i \ln(Q_i) + \sum_{i=1}^{N} P_i \ln(P_i) \\ &= H(P,Q) - H(P), \end{aligned} \tag{3.38}$$

where $H(P,Q)$ is the *cross-entropy* between P and Q and $H(P)$ is the entropy of P. We emphasize that all of these properties of the lattice are purely *geometric*; they do not involve particle strengths $\vec{\Gamma}$ the way the Hamiltonian energy of the lattice does. We mention in connection with this discussion the recent development of information theoretic tools for quantifying predictability in geophysical models. See the recent text of Majda and Wang (2006) and references therein. See also Lim and Nebus (2006) for uses of Monte Carlo simulations in this context.

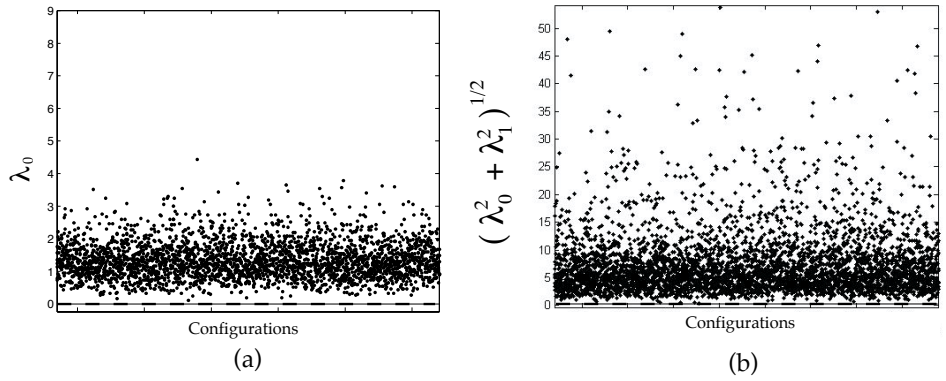

Fig. 4.1 10,000 *configurations of* $N = 10$ *points placed randomly in the plane. Note that none of the values are zero.* (a) *Smallest singular value.* (b) *Sum of squares of the two smallest singular values.*

4. Formation in a Random Environment. Consider the problem of depositing N points at random in the plane. What is the probability that there is *some* choice of $\vec{\Gamma}$ for which the configuration will be an equilibrium? It is a well-known theorem of linear algebra (see Golub and Van Loan (1996), or Lax (2007) for general background) that the set of full-rank matrices is dense in $\mathbb{R}^{M\times N}$, while the set of rank-deficient matrices is not. This might lead one to believe that the chances are small, at best, of finding a rank-deficient matrix corresponding to an equilibrium, which of course is a subset of the set of all rank-deficient matrices. In fact, as we know from the example of rational and irrational numbers on the real line, which are "mutually dense" (between any two rationals is an irrational and between any two irrationals is a rational), even finding an element from a dense set can be challenging using a random search. A dart, assuming it lands on the real line and has a infinitely small point, will be much more likely to land on an irrational number than a rational. In a measure theoretic sense, the rationals form a set of measure zero, while the irrationals form a set of full measure. So, how likely is it that N randomly deposited points in $\mathbb{R}^2$ will produce a rank-deficient configuration matrix? Shown in Figure 4.1 are the smallest singular values associated with 10,000 configurations of $N = 10$ points placed randomly in the plane. Figure 4.1(a) shows the smallest singular value, and Figure 4.1(b) the sum of squares of the two smallest to check whether any of these random configurations has one- or two-dimensional nullspaces—the answer is no. Rank-deficient configuration matrices are hard to produce by the computational equivalent of throwing darts. Indeed, finding them this way is probably not too different than finding a needle in a haystack.[8]

4.1. Brownian Ratchet Scheme. A good way of finding a needle in a haystack is to use a method based on random walks, but random walks with a purpose. The advantage of a Brownian motion–driven algorithm, over say a gradient method, is that all portions of the configuration landscape are sampled in an unbiased way. We describe what we call a Brownian "ratchet" scheme, used in Newton and Chamoun (2007) to uncover new classes of equilibria. The idea behind a Brownian ratchet is

[8] A recent result of Hampton and Moeckel (2006, 2009) shows that the number of stationary configurations for $N = 4$ is finite.

simple—it is a device that sits in a heat bath and rectifies the nonequilibrium thermal fluctuations to generate motion in a preferred direction. Originally conceived of by Feynman (see Feynman, Leighton, and Sands (1966, Chapter 46)), Brownian ratchets are devices which, at the microscopic level, allow motion in one direction and block it in others so that net displacement occurs. Feynman first discussed a paradoxical ratchet device that seemed to extract work from equilibrium thermal fluctuations, in violation of the second law of thermodynamics. However, he also showed that such a device, when reduced to microscopic size, causes fluctuations of the ratchet that are equally likely to occur in either direction. It is now realized that many known biological systems, or so-called motor protein devices, use the surrounding energy associated with unoriented nonequilibrium fluctuations to produce directed motion by employing a potential with ratchet-like features. One can read surveys in Doering (1995, 1998) and Reimann (2002).

In analogy with these studies, we "ratchet" the Brownian motion of the particles, allowing it only in the direction that decreases the smallest singular value (or sum of the smallest k singular values) of A until it drops below a preassigned threshold. In this way we drive the configuration toward an equilibrium[9] (i.e., one or more zero singular values), but we don't know which values to assign $\vec{\Gamma}$ until we derive a basis set for the nullspace of A corresponding to the converged state. The number of singular values that are simultaneously driven to zero corresponds to the dimension of the nullspace and thus determines whether or not the equilibrium configuration is unique (up to a multiplicative constant) with respect to the choice of $\vec{\Gamma}$.

The scheme proceeds with five simple steps:

1. Randomly deposit N points in the plane in an unbiased way and compute the N singular values of the configuration matrix A. These can be ordered and denoted $\sigma_1 \equiv \sigma_{(\max)} \geq \sigma_2 \geq \cdots \geq \sigma_N \equiv \sigma_{(\min)} \geq 0$. The minimum singular value, σ_N, is positive, with probability one.
2. Allow each of the N points to execute an unbiased random walk in $\mathbb{R}^2$, and compute the singular values of A at each step. At each step n, choose a radial variable $r^{(n)} \in [0,1]$ and an angle variable $\theta^{(n)} \in [0, 2\pi]$ drawn from a uniform distribution and scale the radial variable by the smallest singular value associated with the configuration matrix at that step, i.e., $\sigma^{(n)}$ (so the step size decreases as we get closer to a converged state), and move the particle from point $(r^{(n-1)}, \theta^{(n-1)})$ to $(r^{(n)}, \theta^{(n)})$.
3. To find a configuration with a one-dimensional nullspace, at the $(n+1)$st step, keep the new arrangement if the minimal singular value decreases from that of the previous step, i.e., if $\sigma_{(\min)}^{(n+1)} < \sigma_{(\min)}^{(n)}$. Otherwise, discard the configuration, produce a new random arrangement, and repeat this step. For equilibria with k-dimensional nullspaces, drive the scalar quantity $\delta_k \equiv \sqrt{(\sigma_N^{(n)})^2 + \cdots + (\sigma_{N-k+1}^{(n)})^2}$ to zero in a similar fashion.
4. When $\sigma_N^{(n+1)}$ (or equivalently δ_k) is below a certain predetermined threshold, i.e., $\delta_k < \delta_{\text{threshold}}$, the algorithm has converged.
5. Calculate a basis set for the nullspace of A to obtain $\vec{\Gamma}$ and all other properties of the lattice, using both A and $\mathcal{H}$.

The random-walk algorithm is depicted schematically in Figure 4.2. Convergence curves based on this method are shown in Figure 4.3, which depicts the smallest

[9] Although the ratchet mechanism is not dissipative, it provides the same service of driving the system toward an equilibrium, but not necessarily a stable one.

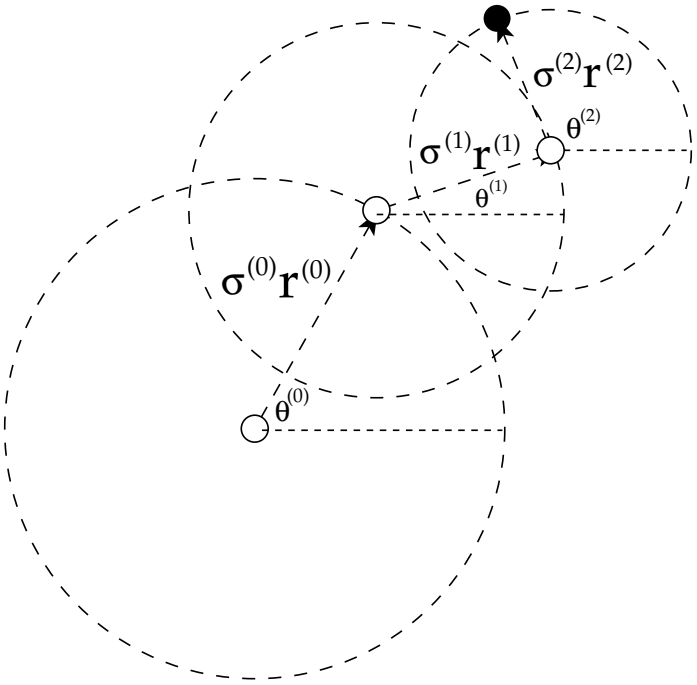

Fig. 4.2 *The random-walk algorithm at the nth step is based on choosing an angle variable* $\theta^{(n)} \in [0, 2\pi]$ *and a radial variable* $r^{(n)} \in [0, 1]$*, both from a uniform distribution, scaled with the size of the smallest singular value,* $\sigma^{(n)}$*, of the configuration matrix at that step.*

singular value as a function of the step number for converged equilibria for $N = 6, 8, 10$. An actual convergence path in the plane of one of the vortices making up the equilibrium is shown in Figure 4.4. We note that, in practice, the method has worked well and has uncovered new classes of equilibrium patterns (see Newton and Chamoun (2007) for examples). Of course, the method doesn't always converge and can sometimes get stuck, for various reasons that need to be better understood. In this context, we mention the importance of developing *constrained* Brownian search schemes, where the vortex strengths are predetermined. For example, within the set of all equilibrium configurations for a given N, it would be particularly desirable to identify those configuration matrices having $\vec{\Gamma} = (1, 1, 1, \ldots, 1)$ in their nullspace.

4.2. Maximum Entropy Theory. Particularly interesting is the fact that the vast majority of patterns found using this method have no discernible symmetry properties at all. As an example, we show in Figure 4.3(b) a converged state, for $N = 10$, along with the paths of each of the particles on the road to the final state. This observation is quite curious given the fact that the overwhelming number of known examples of equilibria so far documented in the literature (those shown in Figure 1.11 would be excellent representative examples) have very distinct symmetries. Why is this the case?

There are two possible explanations for this. Since a Brownian motion–based scheme should, in a sense, find any existing equilibrium with equal probability, it may be that asymmetric equilibrium patterns are far more prevalent than symmetric ones. This is complicated by the fact that the converged states might be influenced by the pool of initial states which creates them, and since these initial states are chosen by a random deposition of points in the plane, asymmetric initial configurations are

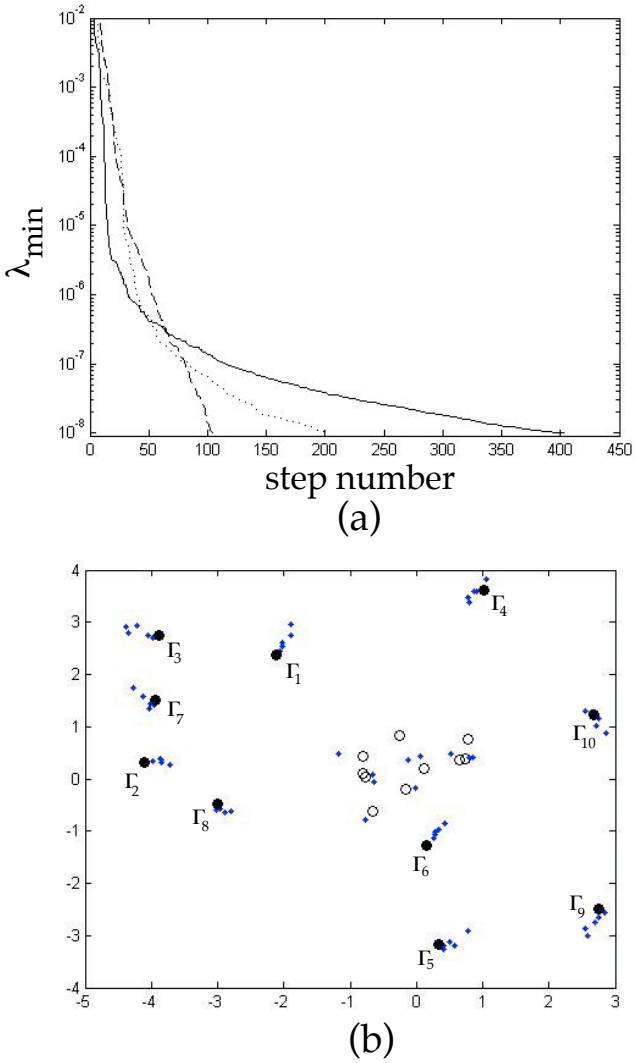

Fig. 4.3 (a) *Convergence of the smallest singular value via the random-walk algorithm:* $N = 6$ *(dashed),* $N = 8$ *(dotted),* $N = 10$ *(solid).* (b) *Convergence of the collection of particles in configuration space toward the final lattice. Unfilled circles represent the initial positions, filled circles represent the converged states, and smaller dots represent some intermediate steps toward convergence.*

overwhelmingly more likely to be produced than symmetric ones, which may bias the pool of converged states to favor asymmetric ones as well.

The second (perhaps related) possibility is that asymmetric states, on average, have higher Shannon entropy than symmetric ones. All other things being equal, this would make them more likely to be picked out at random, since a higher entropy configuration can be produced by a far greater number of microscopic arrangements than a lower entropy state. Phrased differently, a state of lower entropy has preferential clustering of energy among its singular values, while a higher entropy state has more

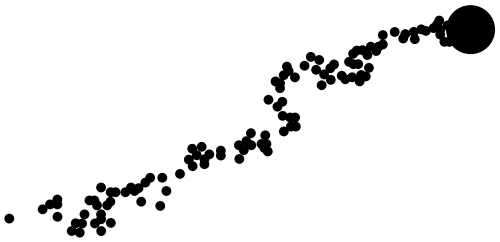

Fig. 4.4 *The configuration path toward convergence of one of the particles making up the lattice.*

even distribution among the modes. Preferential clustering, from a combinatorial perspective, should be less likely than nonpreferential clustering. Hence, the square without the central vortex would be a more likely state than one with the central vortex, since it has higher entropy. Consider the two examples discussed in section 3.4, one with maximal entropy, log(N), and one with minimum entropy 0. For a given N, imagine all possible arrangements of N balls in N bins, each bin representing one of the singular values and the number of balls in a bin determining the size of that singular value. There are exactly N arrangements of balls that are clustered in one bin, since the first could be put in any of the N bins, while the second and remaining balls must be placed in that same bin. On the other hand, there are $N!$ arrangements that will have exactly one ball per bin, hence an even distribution among the modes. This is because the first could be in any of the N bins, the second could be in any of the remaining $N-1$ bins, and so on, with the last forced to be in the final bin. The probability of picking either of these two arrangements out of the full set of all possible arrangements is just the previous number divided by the total number of possible arrangements, which is N^N. Thus, the probability of picking such a *maximum entropy* state at random would be $\frac{N!}{N^N}$, a far higher probability (particularly as $N \to \infty$) than the minimum entropy arrangement, which is $\frac{N}{N^N} = N^{1-N}$. This argument, of course, assumes for simplicity that each of the microscopic arrangements (in this case the distribution of balls in bins) is equally likely to occur. If this is not the case, the probabilities would have to be weighted accordingly, which only muddies the water. Whether or not this analogy is at the bottom of why asymmetric states seem easier to find than symmetric ones would need to be explored by more systematic studies of singular value distributions and entropy levels of asymmetric versus symmetric states.

Our suspicion is that both of these explanations are partially responsible for why most of our converged configurations are asymmetric.[10] The fact that *symmetric* states are far more prevalent in the literature might well be for the same reason that a man looking for his lost keys at night first chooses to look under the street lamp—that is where the light shines!

4.3. Approximate Equilibria. How far is one of the randomly chosen configurations used to produce Figure 4.1 from an actual equilibrium? The answer to this question would give insights into the average spacing between equilibria. If we denote the corresponding "random" full-rank configuration matrix A_0, then we can certainly

[10] In most of the previous studies, all of the vortex strengths are equal, which may also bias the pool in favor of symmetric states over asymmetric ones, although we do know from Aref and Vainchtein (1998) that even with equal strength vortices, it is possible to create an asymmetric lattice.

quantify the distance between it and any given equilibrium with configuration matrix A_1 by calculating the Frobenius norm or 2-norm difference between the two matrices, $\|A_0 - A_1\|_F$. But what is the closest equilibrium? In other words, we would like to minimize this Frobenius norm difference over the set of *all* configuration matrices A_1 with nontrivial nullspaces, which is more challenging. However, consider the following construction. We know that if the rank of a given matrix A is r, then there are r nonzero singular values ordered so that $\sigma^{(1)} \geq \cdots \geq \sigma^{(r)} > \sigma^{(r+1)} = \sigma^{(r+2)} = \cdots = \sigma^{(N)} = 0$ and one obtains the following representation of the matrix A:

$$A = \sigma^{(1)}\mathbf{u}^{(1)}\mathbf{v}^{(1)T} + \sigma^{(2)}\mathbf{u}^{(2)}\mathbf{v}^{(2)T} + \cdots + \sigma^{(r)}\mathbf{u}^{(r)}\mathbf{v}^{(r)T}. \tag{4.1}$$

In this way, the SVD expresses A as a sum of r rank-one matrices. This provides another interpretation of the Shannon entropy of a lattice. Lower entropy lattices have configuration matrices that are closer to matrices of low rank, while higher entropy ones are closer to matrices of full rank. In addition, (4.1) provides an optimal method of approximating A by another matrix of reduced rank. In particular, we can define a rank $k < r$ approximation to A by keeping only the first k terms of (4.1):

$$A_k = \sigma^{(1)}\mathbf{u}^{(1)}\mathbf{v}^{(1)T} + \sigma^{(2)}\mathbf{u}^{(2)}\mathbf{v}^{(2)T} + \cdots + \sigma^{(k)}\mathbf{u}^{(k)}\mathbf{v}^{(k)T} \neq A. \tag{4.2}$$

This matrix is sometimes referred to as the k-truncated SVD. It can be proven that A_k is the optimal reduced rank approximation to the matrix A, meaning that any other rank-k matrix approximation to A has greater error, as measured by their Frobenius-norm difference. The construction (4.1) is reminiscent of a Fourier series representation of a periodic function on an interval in terms of its Fourier modes, where the singular values play the role of the Fourier coefficients providing the appropriate weighting of the modes. The optimality of the linear superposition provided by (4.2) is analogous to the standard fact that the partial sum representation of a Fourier series gives the least-squares error. Therefore, for any randomly chosen full-rank matrix, we can construct the closest matrix to it with any size nullspace we choose, and then calculate the basis set for the nullspace. While such a configuration might not be an exact equilibrium since there is no guarantee that the k-truncated SVD construction would produce a matrix satisfying the constraints of (3.2), one could say that it represents an *optimally approximate* configuration. The vortex strengths would lie in the nullspace of the matrix that is optimally close to this randomly chosen matrix. Whether or not this construction proves to be useful remains to be seen, but the general question of finding "the nearest equilibrium" with specified characteristics (i.e., energy or entropy values, or nullspaces of a particular dimension and span) to any other equilibrium is certainly an interesting and potentially important one.

4.4. Lattice Defects via Matrix Perturbation Theory. Lattice structures with the kinds of line and grain boundary defects shown in Figure 1.6 offer particular challenges. Physically, they arise from a system's attempt to lower its energy in response to external stress, such as the type shown in Figure 1.5, or perhaps because of a change in stability of the current state. For one reason or other, the system of interacting particles seeks a better (i.e., lower energy or more robust) option available to it, and sometimes the best available option is a pattern with broken symmetry. Using matrix perturbation theory, one could frame the problem as follows. Imagine a symmetric lattice with configuration matrix $A_0 \in \mathbb{R}^{M\times N}$ and particle strength vector $\vec{\Gamma}_0 \in \mathbb{R}^N$. Suppose a "nearby" lattice exists having configuration matrix $A_\epsilon \in \mathbb{R}^{M\times N}$

and particle strength vector $\vec{\Gamma}_\epsilon \in \mathbb{R}^N$. Let

$$A_\epsilon \equiv A_0 + A_1, \quad \text{where} \quad A_1 \equiv (A_\epsilon - A_0), \tag{4.3}$$

$$\vec{\Gamma}_\epsilon \equiv \vec{\Gamma}_0 + \vec{\Gamma}_1, \quad \text{where} \quad \vec{\Gamma}_1 \equiv (\vec{\Gamma}_\epsilon - \vec{\Gamma}_0). \tag{4.4}$$

Assume further that the "defect" lattice is indeed a perturbation of the symmetric lattice, i.e.,

$$\frac{\|A_1\|_F}{\|A_0\|_F} \sim \epsilon \ll 1, \quad \frac{\|\vec{\Gamma}_1\|}{\|\vec{\Gamma}_0\|} \sim \epsilon \ll 1. \tag{4.5}$$

Given an allowable unperturbed state $A_0\vec{\Gamma}_0 = 0$, how does one find a nearby perturbed state $A_\epsilon\vec{\Gamma}_\epsilon = 0$? From (4.3) and (4.4) we have

$$(A_0 + A_1)(\vec{\Gamma}_0 + \vec{\Gamma}_1) = 0. \tag{4.6}$$

Using the ordering imposed by (4.5) yields

$$O(1): \quad A_0\vec{\Gamma}_0 = 0, \tag{4.7}$$

$$O(\epsilon): \quad A_0\vec{\Gamma}_1 = -A_1\vec{\Gamma}_0, \tag{4.8}$$

$$O(\epsilon^2): \quad A_1\vec{\Gamma}_1 = 0. \tag{4.9}$$

The first of these equations (4.7) defines both A_0 and $\vec{\Gamma}_0$ associated with the defect-free state (symmetric). Then, by the Fredholm alternative theorem, (4.8) requires

$$-A_1\vec{\Gamma}_0 \perp Null(A_0^T). \tag{4.10}$$

This defines the matrix A_1 in terms of A_0 and $\vec{\Gamma}_0$. Equation (4.9) then tells us that

$$\vec{\Gamma}_1 \in Null(A_1), \tag{4.11}$$

which, together with (4.8), defines $\vec{\Gamma}_1$. The "defect" state thus constructed is defined by A_ϵ and $\vec{\Gamma}_\epsilon$. More restrictively, if we require that the particle strengths of the defect-free state and the perturbed state be the same, then $\vec{\Gamma}_1 = 0$, which by (4.8) implies

$$\vec{\Gamma}_0 \in Null(A_1). \tag{4.12}$$

For a nontrivial solution to exist, the nullspaces of A_0 and A_1 must have some vectors in common and $\vec{\Gamma}_0$ must lie in both subspaces. To bring in the additional feature that the defect state resides at lower energy, one also would need to require that the perturbed energy (2.12) be lower than the unperturbed energy, i.e., $\mathcal{H}_\epsilon < \mathcal{H}_0$, a condition that involves both the particle configuration and particle strengths.

4.5. Optimal Mesh Generation. The techniques discussed in this article can be used to generate finite-element meshes on general surfaces if you think of each vertex in the mesh as a particle and execute the Brownian ratchet scheme so that

the particles evolve to a lattice that optimizes some quantity. We focus on constructing meshes on the sphere, but constructing meshes on more complex (nonconstant curvature) surfaces such as the body of an airplane, a human skull, or the cavity of a pulsating heart are of obvious interest and one can find an interesting recent overview of relevant methods in the book of Edelsbrunner (2006). In fact, using interacting particle systems to perform meshing is an active area of research in the computer graphics community (see, for example, Szeliski, Tonnesen, and Terzopoulos (1993), Witkin and Heckbert (1994), and Chouraqui and Elber (1996)). The question of how one generates a mesh that is in some sense optimal is related to the question of how one distributes N points uniformly on a surface, particularly for large N. On the sphere, despite the fact that the problem has a long history, dating back to J.J. Thomson's 1904 formulation associated with his "plum-pudding" model of the atom (an equally unsuccessful follow-up to the ill-fated vortex-atom theory of matter), there is no known general solution, and it is listed as Problem 7 on Smale's "Mathematical Problems for the Next Century" (2000). This question is of practical importance since a uniform distribution of points on a sphere is typically needed for the purposes of numerical integration. One example is in the analysis of satellite data from the earth's surface, where it is usually necessary to approximate integrals over the sphere (or perturbed sphere) by arithmetic averages at some judiciously chosen set of points. In this case, one would like to choose the set of points $\{x_1, \ldots, x_N\}$ so that for a large class of smooth functions $f(x)$, the difference

$$\left| \frac{1}{4\pi} \int_{S^2} f(x) d\sigma(x) - \frac{1}{N} \sum_{j=1}^{N} f(x_j) \right| \tag{4.13}$$

is as small as possible. Here, $\sigma(x)$ is the Lebesgue measure on the sphere. A related notion is the construction of spherical t-designs of Hardin and Sloane (1996). There are other physical models which rely on optimal distributions of points on the sphere, such as the arrangement of the protein subunits of a protein coat of a spherical virus (see Casper and Klug (1962)), the arrangement of atoms in a spherical molecule such as the buckminsterfullerine molecule (Kroto et al. (1985), Kroto (1987)) and the vortex distributions in thin film superconductors with spherical geometry (Dodgson (1996)) or on more general curved surfaces of nonconstant curvature where one might want to study quantum Hall effects (Dodgson and Moore (1997)). The problem is closely related to the so-called Tammes problem of determining the largest diameter that N equal circles (i.e., spherical caps) can have when packed onto the surface of a sphere, without any overlapping. Alternatively, if the center of each circle is the vertex of a polyhedron, find the polyhedron that maximizes the shortest edge lengths. This "spherical packing" problem was originally formulated and studied by the biologist Tammes (1930) in connection with his study of the pattern of orifices in spherical pollen grains and has since spawned a large literature. An overview of optimal solutions for certain ranges of N is provided in Clare and Kepert (1986), while a particularly comprehensive and rapidly evolving database of "empirical" global minima for a whole host of molecular clusters can be found at the Cambridge Cluster Database: http://www-wales.ch.cam.ac.uk/CCD.html. We mention that in one dimension, the corresponding problem of how to place particles on a line so that they form an equilibrium has been solved (and related to the location of zeros of certain classical functions), and is reviewed nicely in Aref (2007a) and discussed in Hardin and Saff (2004).

Consider N equal point charges on the surface of a unit conducting sphere. How does one distribute these points so that the Coulomb energy E_1,

$$E_1 = \sum_{i=1}^{N} \sum_{j=1}^{N}{}' \frac{1}{|z_i - z_j|}, \tag{4.14}$$

is minimized? The points that globally minimize this quantity are called Fekete points and one can pose this problem on more complex surfaces. More generally, we can define the Riesz s-energy E_s of a set of N distinct points $\omega_N = \{x_i\}_1^N$ as

$$E_s(\omega_N) = \sum_{i=1}^{N} \sum_{j=1}^{N}{}' |z_i - z_j|^{-s}, \quad s > 0. \tag{4.15}$$

For parameter value $s = 0$, we take it to be the logarithmic interaction; for $s = 1$, it is the Coulomb energy E_1; while for $s \to \infty$, with N fixed, (4.15) is increasingly dominated by the terms involving the smallest pairwise distances, which leads to the best-packing problem (see Hardin and Saff (2004) for a comprehensive discussion of the results in this field). Alternatively and perhaps more immediately relevant are points that *maximize* the product of all the interparticle distances

$$\Pi_{i=1,j=1}^{N}{}' |z_i - z_j|, \tag{4.16}$$

which is equivalent to *minimizing* the interparticle energy

$$E_0 = \sum_{i=1}^{N} \sum_{j=1}^{N}{}' \log \frac{1}{|z_i - z_j|}, \tag{4.17}$$

i.e., the Hamiltonian (2.12). These points are called logarithmic extreme points, or elliptic Fekete points. For example, it is obvious that for $N = 2$, the optimal distribution is the antipodal points, but it is less obvious that, for $N = 8$, as an example, the optimal configuration is not the cube, but a twisted noncubic rectangular parallelepiped (see Wille (1986)), and for $N \leq 12$, icosahedral based lattices form minimum energy configurations. It is certainly known that optimal solutions (particularly for large N) are not necessarily the ones with greatest symmetry (Bergersen, Boai, and Palffy-Muhoray (1994)). While there is no known general solution to the problem, optimal configurations are known for values of N in the range (roughly) $2 \leq N \leq 100$ and for other special values of N. As N increases, solid information becomes scant until one reaches the asymptotic regime ($N \to \infty$), where the fog clears and a whole host of viable techniques emerges. The article of Saff and Kuijlaars (1997) is a nice introduction to this regime. What makes the problem difficult for finite (but large) N is that the number of local minima increases exponentially with N and that these local minima congregate in close proximity to the global minimum in many cases (see Erber and Hockney (1991), Glasser and Every (1992), or Morris, Deaven, and Ho (1996)), making analytical formulas for energy levels (as in Aref (2007c) for the planar problem) particularly valuable.

In general terms, configurations that try to organize the particles in regular hexagonal tilings of the sphere are typically optimal. The problem is that the Euler characteristic formula $F - E + V = 2$, where F is the number of faces, E is the number of edges, and V is the number of vertices, rules this out. So, the particles try to "perturb" these configurations in some way that the Euler formula is respected, and this

often (but not always) involves creating pentagons (see Altschuler et al. (1997, 2005, 2006)). The effect is that defects or "disclinations" form on the spherical surface (see Edmundson (1992), Wales and Ulker (2006)) when N is sufficiently large ($N \sim 300$). In fact, any tiling of the sphere that consists exclusively of hexagons and pentagons must have exactly 12 pentagons (3 edges emanating from each vertex). For example, the soccer ball pattern, or truncated icosahedron (whose dual structure made up of carbon atoms at the vertices is the C_{60} buckyball molecule), for $N = 32$ has 12 pentagonal and 20 hexagonal faces (Kroto et al. (1985)).

Systematic studies of how to distribute points on a sphere based on geometric iteration have been carried out and properties of lattices based on procedures such as icosahedral dissection (Baumgardner and Frederickson (1985)) are understood. Start with an icosahedral configuration with a particle placed at each vertex, place a new particle at the midpoint of each edge projected on the sphere, and continue with this process of placing new particles at the midpoints of the geodesic segments connecting previous vertices. One can see that on the kth dissection, there are exactly $2 + 10(k + 1)^2$ nodes. Measures of the uniformity of theses meshes as $k \to \infty$ can be obtained. See Cui and Freeden (1997) for comparisons of five different schemes based on the concept of generalized discrepancy. Another procedure (see Saff and Kuijlaars (1997)) that produces lattices with spiral structure seems to have some advantages over icosahedral dissection (Rakhmanov, Saff, and Zhou (1994)). We now have a full decomposition of all the Platonic solid equilibria on the sphere (see Jamaloodeen and Newton (2006)); however, research into the energy and entropy landscapes associated with them and their general use as building blocks for more complex lattices has not been completed.

5. Computational Challenges. The numerical challenges associated with the methods described in this paper stem from the fact that as the particles home in on an equilibrium, the configuration matrix A is rank deficient, and the resulting numerical problem $A\vec{\Gamma} = 0$ is ill-posed (see Hansen (1998) or Demmel (1997)). This is because near an equilibrium with nullspace dimension $m < N$, there is a cluster of extremely small singular values, with a well-separated gap between the smallest and largest singular values, making the condition number of A very large. Since the condition number associated with a matrix measures the system sensitivity to round-off errors, this is bad news. Often, a large condition number associated with a matrix indicates an incorrect or an incomplete mathematical model and one must go back to first principles and modify the model—this is most definitely not the case here. It is precisely the configurations with "infinite condition number" (i.e., $\sigma_{\max}/\sigma_{\min} \to \infty$) we seek. Fortunately, these problems are beginning to be well studied, in particular with respect to the algorithms associated with stable, accurate, and fast SVD solvers.

Consider, for example, the relationship between the SVD of A and the eigenvalue decomposition of A^TA. Since $A = U\Sigma V^T$ and $A^T = V\Sigma^T U^T$, we have immediately that $A^TA = V\Sigma^T(U^TU)\Sigma V^T = V\Sigma^T\Sigma V^T$. This implies that we could perform the SVD of A by first forming A^TA. Then (i) compute the eigenvalue decomposition of $A^TA = V\Lambda V^T$; (ii) obtain Σ by defining it to be the M by N nonnegative diagonal square root of the matrix Λ; (iii) solve the system $U\Sigma = AV$ for unitary U via QR factorization. Although this approach is straightforward mathematically, it is well known to be numerically unstable since the eigenvalue problem is extremely sensitive to perturbation. Nevertheless, most algorithms for the computation of the SVD of a general matrix rely, in some way, on the computation of the eigenvalue decomposition of a Hermitian square matrix, but there are both stable and unstable ways of doing

this. We refer the reader to Trefethen and Bau (1997) (particularly Lecture 31) for a lucid introduction to this topic.

In addition, there are cost considerations in selecting an algorithm. For example, the classical algorithm for computing the SVD due to Golub and Kahan (1965) is known to be computationally costly. It is based on the idea of first transforming A into upper bidiagonal form B by a finite sequence of alternating left and right Householder transformations. Then, the QR algorithm is applied implicitly to B^TB making B converge to Σ, while the left and right orthogonal transformations produce U and V. However, the computational price for such an approach, as discussed in Hansen (1998) is that the algorithm needs $14MN^2 + 8N^3$ flops to compute the full SVD, a very high price to pay, particularly if this must be performed at each random-walk step. However, in a sense, all that is necessary at each step is to gain just enough information to know when a configuration produces a rank-deficient pattern. Thus, one can use a far less expensive rank-revealing decomposition (see the discussion in Hansen (1998)) at each random step to check for convergence, then when satisfied that an equilibrium has been located to high enough accuracy, perform a full-scale SVD.

There are a whole host of random number generating algorithms one could choose from, as described in Gentle (2003), or more specifically in L'Ecuyer (2004) and Aiello, Rajagopalan, and Verga (1998), and optimizing these could also improve performance considerably. One thing is certain: MATLAB's rand() algorithm is not the fastest. There are alternatives to using uniformly distributed random numbers at each step as well. For example, one could imagine using the heat kernel as a means of generating the random step not unlike the approach introduced in Chorin (1973) and discussed more generally in Cottet and Koumoutsakos (2000). Alternatively, one could add stochastic forcing terms directly to the dynamical intervortical distance equations (3.2), turning them into Itô equations instead of deterministic ones, as is done, for example, in Agullo and Verga (1997, 2001) and Kevlahan (2005) directly to the equations (2.6) for $N = 2$. All of these possibilities remain to be more fully explored.

6. Discussion and Future Directions. The ultimate payoff of being able to rapidly compute large N lattices includes the possibility of designing them with specific features built in. It is known, for example, that associated with each vortex equilibrium is a specific topological streamline pattern or "template" for the flowfield, which governs the way particles are transported through the structure, collections of particles mix and evolve, and interfaces stretch and deform (see Aref and Brøns (1998), Kidambi and Newton (2000), Newton and Ross (2006), Brøns (2007)). The patterns produced are a delicate kinematic combination of the relative positions of the vortices within the lattice, along with their individual strengths. Since the techniques discussed in this article have the ability to find *all* possible strengths associated with a given pattern, the potential exists to find lattices which optimize these mixing and transport features, an issue that is of general interest in wake patterns generated by collections of bluff bodies or schools of swimming fish. In addition, with the experimental ability to "knock" a given lattice from one fixed state to another by an external "driving force," one could imagine taming these forces for beneficial goals, such as coaxing the system to a new energy state, for example, from the lowest energy state to one of the 17 higher energy states shown in Figure 1.11. Or, for the purposes of optimizing the robustness of the pattern, one could imagine driving the configuration to a higher entropy level.

In many high-dimensional systems with complex energy surfaces, understanding the *geometry* of the energy landscape in the neighborhood of *local minimizers* or

more generally the *local extremizers* may be much more relevant than finding global minimizers of the system. For example, often it is important to ask what is the probability of being captured by an equilibrium, or, once captured, how much energy need be expended to escape to another region of the accessible surface. Both of these questions have much more to do with the shape of the energy surface surrounding the extrema than the actual values of the energy at the minima. Energy landscapes littered with many local minima creating a large basin of attraction, or "catchment region," are much more likely to be captured in a probabilistic sense than a global minimum which may be isolated with a small basin of attraction. In addition, a global minimum sitting in a shallow basin is typically much easier to escape from, hence is less robust than a local minimum surrounded by steep walls. It is the potentially subtle and complicated *geometric features* of the energy and entropy landscapes that are much more revealing than their relative values at extremum points.

We end with a list of ten interesting future research directions associated with the characterization of lattices, which make use of both the geometry of the energy landscape imposed by the Hamiltonian $\mathcal{H}$ and the singular value structure of the configuration matrix A:

1. Understanding the dynamical stability of the vortex lattices for the full set of $\vec{\Gamma}$ in the nullspace of A and uncovering the interplay between the geometry of the Hamiltonian energy landscape and the nullspace structure of A.
2. Developing *constrained* Brownian ratchets, or combined Brownian ratchet and gradient algorithms, that seek configurations with prescribed $\vec{\Gamma}$, with a particular focus on finding and classifying all configurations with matrices having $(1, 1, 1, \ldots, 1)$ in their nullspace.
3. Implementing the Brownian ratchet algorithms on more general surfaces for the purpose of optimal mesh generation.
4. Including boundaries in the configuration matrix approach, particularly for lattice cells with symmetries so that image methods could be used, but also when the boundary breaks the symmetry of the cell.
5. Understanding the singular value distributions of the configuration matrix for particle configurations with discrete symmetries, as compared with those that have no symmetries. How do the Shannon entropies of these two general classes of lattices compare and how do the allowable vortex strengths compare?
6. Constructing configuration matrices for lattices with defects, or dislocations, perhaps via perturbation theory on the underlying defect-free configuration matrix.
7. Understanding the *evolution* of the Shannon entropy associated with a collection of particles as it evolves toward an equilibrium configuration to better understand the role of entropy in the selection of one lattice geometry over another.
8. Using both the Hamiltonian and the Shannon entropy to *design* lattices with specific optimal features built in, such as identifying minimal energy (stable), maximal entropy (robust) lattices.
9. Understanding the effects of changing the monotonic velocity profile associated with each lattice site to more general profiles.
10. Obtaining a full enumeration of the number of equilibria, both stable and unstable.

These are all topics that seem likely to play an increasingly prominent role in future developments and we hope the themes discussed in this article offer readers a fresh and inviting perspective on some fascinating topics in applied mathematics.

Acknowledgments. The first author would like to thank the Mathematics Department at UC Santa Barbara for their hospitality during the winter quarter of 2007 when most of this manuscript was written.

REFERENCES

J.R. Abo-Shaer, C. Raman, J.M. Vogels, and W. Ketterle (2001), *Observation of vortex lattices in Bose-Einstein condensates*, Science, 292, pp. 476–479.

A.A. Abrikosov (1957), *On the magnetic properties of superconductors of the second group*, Sov. Phys. JETP, 5, pp. 1174–1178.

A.A. Abrikosov (2004), *Type II superconductors and the vortex lattice*, Rev. Modern Phys., 76, pp. 975–979.

O. Agullo and A.D. Verga (1997), *Exact two vortices solution of Navier-Stokes equations*, Phys. Rev. Lett., 78, pp. 2361–2364.

O. Agullo and A.D. Verga (2001), *Effect of viscosity in the dynamics of two point vortices: Exact results*, Phys. Rev. E, 63, article 056304.

W. Aiello, S. Rajagopalan, and R. Venkatesan (1998), *Design of practical and provably good random number generators*, J. Algorithms, 29, pp. 358–389.

E.L. Altschuler, T.J. Williams, E.R. Ratner, R. Tipton, R. Stong, F. Dowla, and F. Wooten (1997), *Possible global minimum lattice configurations for Thomson's problem of charges on a sphere*, Phys. Rev. Lett., 78, pp. 2681–2685.

E.L. Altschuler and A. Perez-Garrido (2005), *Global minimum for Thomson's problem of charges on a sphere*, Phys. Rev. E, 71, article 047703.

E.L. Altschuler and A. Perez-Garrido (2006), *Defect free global minima in Thomson's problem of charges on a sphere*, Phys. Rev. E, 73, article 036108.

I.S. Aranson and L. Kramer (2002), *The world of the complex Ginzburg-Landau equation*, Rev. Modern Phys., 74, pp. 99–143.

H. Aref (1982), *Point vortex motions with a center of symmetry*, Phys. Fluids, 25, pp. 2183–2187.

H. Aref (2007a), *Vortices and polynomials*, Fluid Dynam. Res., 39, pp. 5–23.

H. Aref (2007b), *Point vortex dynamics—A classical mathematics playground*, J. Math. Phys., 48, article 065401.

H. Aref (2007c), *A note on the energy of relative equilibria of point vortices*, Phys. Fluids, 19, article 103603.

H. Aref and M. Brøns (1998), *On stagnation points and streamline topology in vortex flows*, J. Fluid Mech., 370, pp. 1–27.

H. Aref, P.K. Newton, M.A. Stremler, T. Tokieda, and D.L. Vainchtein (2003), *Vortex crystals*, Adv. in Appl. Mech., 39, pp. 1–79.

H. Aref and D. Vainchtein (1998), *Asymmetric equilibrium patterns of point vortices*, Nature, 392, pp. 769–770.

H. Aref and M. van Buren (2005), *Vortex triple rings*, Phys. Fluids, 17, article 057104.

J.R. Baumgardner and P.O. Frederickson (1985), *Icosahedral discretization of the two-sphere*, SIAM J. Numer. Anal., 22, pp. 1107–1115.

B. Bergersen, D. Boai, and P. Palffy-Muhoray (1994), *Equilibrium configurations of particles on a sphere: The case of logarithmic interactions*, J. Phys. A, 27, pp. 2579–2586.

F. Bethuel, H. Brezis, and F. Helein (1994), *Ginzburg-Landau Vortices*, Birkhäuser Press, Basel.

M. Brøns (2007), *Streamline topology—Patterns in fluid flows and their bifurcations*, Adv. Appl. Mech., 41, pp. 1–43.

D.A. Butts and D.S. Rokhar (1999), *Predicted signatures of rotating Bose-Einstein condensates*, Nature, 397, pp. 327–329.

L.J. Campbell (1981), *Transverse normal modes of finite vortex arrays*, Phys. Rev. A, 24, pp. 514–534.

L.J. Campbell and R. Ziff (1978), *A Catalog of Two-Dimensional Vortex Patterns*, LA-7384-MS, Rev., Informal report, Los Alamos Scientific Laboratory.

L.J. Campbell and R. Ziff (1979), *Vortex patterns and energies in a rotating superfluid*, Phys. Rev. B, 20, pp. 1886–1902.

D.L.D. Casper and A. Klug (1962), *Proceedings of the Cold Spring Harbor Symposium on Quantitative Biology*, Vol. 27, Cold Spring Harbor Laboratory Press, New York.

A.J. Chorin (1973), *Numerical study of slightly viscous flow*, J. Fluid Mech., 57, pp. 785–796.
P. Chouraqui and G. Elber (1996), *Physically based adaptive triangulation of freeform surfaces*, in Computer Graphics International 1996 (CGI'96), IEEE Computer Society Press, pp. 144–153.
B.W. Clare and D.L. Kepert (1986), *The closest packing of equal circles on a sphere*, Proc. Roy. Soc. London Ser. A, 405, pp. 329–344.
I. Coddington, P. Engels, V. Schweikhard, and E.A. Cornell (2003), *Observation of Tkachenko oscillations in rapidly rotating Bose-Einstein condensates*, Phys. Rev. Lett., 91, article 100402.
G.H. Cottet and P.D. Koumoutsakos (2000), *Vortex Methods: Theory and Practice*, Cambridge University Press, Cambridge, UK.
J. Cui and W. Freeden (1997), *Equidistribution on the sphere*, SIAM J. Sci. Comput., 18, pp. 595–609.
F. Dalfovo, S. Giorgini, L.P. Pitaevskii, and S. Stringari (1999), *Theory of Bose-Einstein condensation on trapped gases*, Rev. Modern Phys., 71, pp. 463–512.
O. Darrigol (2005), *Worlds of Flow: A History of Hydrodynamics from the Bernoullis to Prandtl*, Oxford University Press, New York.
P. Dear (2006), *The Intelligibility of Nature: How Science Makes Sense of the World*, University of Chicago Press, Chicago.
J.W. Demmel (1997), *Applied Numerical Linear Algebra*, SIAM, Philadelphia.
M.J.W. Dodgson (1996), *Investigation on the ground states of a model thin-film superconductor on a sphere*, J. Phys. A, 29, pp. 2499–2508.
M.J.W. Dodgson and M.A. Moore (1997), *Vortices in a thin-film superconductor with a spherical geometry*, Phys. Rev. B, 55, pp. 3816–3831.
C.R. Doering (1995), *Randomly rattled ratchets*, Nuovo Cimento D, 17, pp. 685–698.
C.R. Doering (1998), *Stochastic ratchets*, Phys. A, 254, pp. 1–6.
C.F. Driscoll and K.S. Fine (1990), *Experiments on vortex dynamics in pure electron plasmas*, Phys. Fluids, 2, pp. 1359–1366.
D. Durkin and J. Fajans (2000), *Experiments on two-dimensional vortex patterns*, Phys. Fluids, 12, pp. 289–293.
W. E (1994), *Dynamics of vortices in Ginzburg-Landau theories with applications to superconductivity*, Phys. D, 77, pp. 383–404.
H. Edelsbrunner (2006), *Geometry and Topology for Mesh Generation*, Cambridge University Press, Cambridge, UK.
J.R. Edmundson (1992), *Distribution of point charges on the surface of a sphere*, Acta Cryst., A48, pp. 60–69.
P. Engels, I. Coddington, P.C. Haljan, and E.A. Cornell (2002), *Nonequilibrium effects of anisotropic compression applied to vortex lattices in Bose-Einstein condensates*, Phys. Rev. Lett., 89, article 100403.
P. Engels, I. Coddington, P.C. Haljan, V. Schweikhard, and E.A. Cornell (2003), *Observation of long-lived vortex aggregates in rapidly rotating Bose-Einstein condensates*, Phys. Rev. Lett., 90, article 170405.
T. Erber and G.M. Hockney (1991), *Equilibrium configurations of N equal charges on a sphere*, J. Phys. A, 24, pp. L1369–L1377.
U. Essmann and H. Trauble (1967), *The direct observation of individual flux lines in type* II *superconductors*, Phys. Lett., 24A, pp. 526–530.
A.L. Fetter, P.C. Hohenberg, and P. Pincus (1966), *Stability of a lattice of superfluid vortices*, Phys. Rev., 147, pp. 140–152.
R.P. Feynman (1955), in *Progress in Low Temperature Physics*, D.F. Brewer, ed., North–Holland, Amsterdam, Vol. 1, Chapter 11.
R.P. Feynman, R.B. Leighton, and M. Sands (1966), *The Feynman Lectures on Physics, Vol.* 1, Addison-Wesley, Reading, MA.
K.S. Fine, A.C. Cass, W.G. Flynn, and C.F. Driscoll (1995), *Relaxation of* $2D$ *turbulence to vortex crystals*, Phys. Rev. Lett., 75, pp. 3277–3280.
J.E. Gentle (2003), *Random Number Generation and Monte Carlo Methods*, 2nd ed., Springer-Verlag, New York.
L. Glasser and A.G. Every (1992), *Energies and spacings of point charges on a sphere*, J. Phys. A, 25, pp. 2473–2482.
V.L. Ginzburg and L.D. Landau (1950), *On the theory of superconductivity*, Zh. Eksp. Theor. Fiz., 20, pp. 1064–1082.
G.H. Golub and C. F. Van Loan (1996), *Matrix Computations*, 3rd ed., Johns Hopkins University Press, Baltimore, MD.
G.H. Golub and W. Kahan (1965), *Calculating the singular values and pseudo-inverse of a matrix*, SIAM J. Numer. Anal., 2, pp. 205–224.
B.A. Grzybowski, H.A. Stone, and G.M. Whitesides (2000), *Dynamic self-assembly of magnetized, millimeter-sized objects rotating at a liquid-air interface*, Nature, 405, pp. 1033–1036.

S. Gueron and I. Shafrir (1999), *On a discrete variational problem involving interacting particles*, SIAM J. Appl. Math., 60, pp. 1–17.
M. Hampton and R. Moeckel (2006), *Finiteness of relative equilibria of the four-body problem*, Invent. Math., 163, pp. 289–312.
M. Hampton and R. Moeckel (2009), *Finiteness of stationary configurations of the four-vortex problem*, Trans. Amer. Math. Soc., 361, pp. 1317–1332.
P.C. Hansen (1998), *Rank-Deficient and Discrete Ill-Posed Problems: Numerical Aspects of Linear Inversion*, SIAM Monogr. Math. Model. Comput. 4, SIAM, Philadelphia.
R.H. Hardin and E.B. Saff (2004), *Discretizing manifolds via minimum energy points*, Notices Amer. Math. Soc., 51, pp. 1186–1194.
R.H. Hardin and N.J.A. Sloane (1996), *McLaren's improved snub cube and other new spherical designs in three dimensions*, Discrete Comput. Geom., 15, pp. 429–441.
T.H. Havelock (1931), *The stability of motion of rectilinear vortices in ring formation*, Philos. Mag., 11, pp. 617–633.
H.F. Hess, R.B. Robinson, R.G. Dynes, J.M. Valles Jr., and J.V. Waszczak (1989), *Scanning-tunneling microscope observation of the Abrikosov flux lattice and the density of states near and inside a fluxoid*, Phys. Rev. Lett., 62, pp. 214–216.
H. Hotelling (1933), *Analysis of a complex of statistical variables into principal components*, J. Educ. Psych, 24, pp. 417–441, 498–520.
M.I. Jamaloodeen and P.K. Newton (2006), *The N-vortex problem on a rotating sphere.* II. *Heterogeneous Platonic solid equilibria*, Proc. R. Soc. Lond. Ser. A, 462, pp. 3277–3299.
R.L. Jerrard and H.M. Soner (1998), *Dynamics of Ginzburg–Landau vortices*, Arch. Rational Mech. Anal., 142, pp. 99–125.
D.Z. Jin and D.H.E. Dubin (1998), *Two-dimensional vortex crystals*, Ann. New York Acad. Sci., 848, pp. 18–25.
D.Z. Jin and D.H.E. Dubin (2000), *Characteristics of two-dimensional turbulence that self-organizes into vortex crystals*, Phys. Rev. Lett., 84, pp. 1443–1446.
J.B. Keller (1962), *Factorization of matrices by least-squares*, Biometrika, 49, pp. 239–242.
N.K.R. Kevlahan (2005), *Stochastic differential equation models of vortex merging and reconnection*, Phys. Fluids, 17, article 065107.
P.G. Kevrekidis, R. Carretero-Gonzalez, D.J. Frantzeskakis, and I.G. Kevrekidis (2004), *Vortices in Bose-Einstein condensates: Some recent developments*, Modern Phys. Lett. B, 18, pp. 1481–1505.
R. Kidambi and P.K. Newton (2000), *Streamline topologies for integrable vortex motion on a sphere*, Phys. D, 140, pp. 95–125.
M. Kirby (2001), *Geometrical Data Analysis: An Empirical Approach to Dimensionality Reduction and the Study of Patterns*, John Wiley & Sons, New York.
H. Kragh (2002), *The vortex atom: A Victorian theory of everything*, Centaurus, 44, pp. 32–114.
H.W. Kroto, J.R. Heath, S.C. O'Brien, R.F. Curl, and R.E. Smalley (1985), C_{60}*: Buckminsterfullerine*, Letters to Nature (London), 318, pp. 162–163.
H.W. Kroto (1987), *The stability of the fullerines* C_n *with* $n = 24, 28, 32, 36, 50, 60$ *and* 70, Letters to Nature (London), 328, pp. 529–531.
S. Kullback and R. A. Leibler (1951), *On information and sufficiency*, Ann. Math. Statist., 22, pp. 79–86.
P. L'Ecuyer (2004), *Random number generation*, in Handbook of Computational Statistics, J.E. Gentle, W. Haerdle, and Y. Mori, eds., Springer-Verlag, Berlin, pp. 35–70.
I.M. Lansky and T.M. O'Neil (1997), *Stability analysis of a two-dimensional vortex pattern*, Phys. Rev. E, 55, pp. 7010–7014.
P.D. Lax (2007), *Linear Algebra and Its Applications*, 2nd ed., Wiley, New York.
A.J. Leggett (2001), *Bose-Einstein condensation in the alkali gases: Some fundamental concepts*, Rev. Modern Phys., 73, pp. 307–356.
D. Lewis and T. Ratiu (1996), *Rotating n-gon/kn-gon vortex configurations*, J. Nonlinear Sci., 6, pp. 385–414.
C. Lim and J. Nebus (2006), *Vorticity, Statistical Mechanics and Monte Carlo Simulations*, Springer Monogr. Math., Springer-Verlag, New York.
F.-H. Lin (1996), *Some dynamical properties of Ginzburg-Landau vortices*, Comm. Pure Appl. Math., 49, pp. 323–359.
F.-H. Lin (1998), *Complex Ginzburg-Landau equations and dynamics of vortices, filaments, and codimension-2 submanifolds*, Comm. Pure Appl. Math., 51, pp. 385–441.
A.J. Majda and X. Wang (2006), *Nonlinear Dynamics and Statistical Theories for Basic Geophysical Flows*, Cambridge University Press, Cambridge, UK.
J.C. Maxwell (1965), *On physical lines of force* (1861), reprinted in The Scientific Papers of James Clerk Maxwell, W.D. Niven, ed., Dover, New York.

A.M. Mayer (1878), *Floating magnets*, Nature, 17, pp. 487–488.
V.V. Meleshko and H. Aref (2007), *A bibliography of vortex dynamics* 1858–1956, Adv. Appl. Mech., 41, pp. 197–292.
G.J. Mertz (1978), *Stability of body-centered polygonal configurations of ideal vortices*, Phys. Fluids, 21, pp. 1092–1095.
J.R. Morris, D.M. Deaven, and K.M. Ho (1996), *Genetic algorithm energy minimization for point charges on a sphere*, Phys. Rev. B, 53, pp. R1740–R1743.
J. Neu (1990), *Vortex dynamics of complex scalar fields*, Phys. D, 43, pp. 385–406.
P.K. Newton (2001), *The N-Vortex Problem: Analytical Techniques*, Appl. Math. Sci. 145, Springer-Verlag, New York.
P.K. Newton and G. Chamoun (2007), *Construction of point vortex equilibria via Brownian ratchets*, Proc. R. Soc. Lond. Ser. A, 463, pp. 1525–1540.
P.K. Newton and S.D. Ross (2006), *Chaotic advection in the restricted four-vortex problem on a sphere*, Phys. D, 223, pp. 36–53.
L. Peres and J. Rubinstein (1993), *Motion of vortex lines in $U(1)$ Ginzburg-Landau models*, Phys. D, 64, pp. 299–309.
L.M. Pismen and J. Rubinstein (1991), *Motion of vortex lines in the Ginzburg-Landau model*, Phys. D, 47, pp. 353–360.
E.A. Rakhmanov, E.B. Saff, and Y.M. Zhou (1994), *Minimal discrete energy on the sphere*, Math. Res. Lett., 1, pp. 647–662.
P. Reimann (2002), *Brownian motors: Noisy transport far from equilibrium*, Phys. Rep., 361, pp. 57–265.
E.B. Saff and A.B.J. Kuijlaars (1997), *Distributing many points on a sphere*, Math. Intell., 19, pp. 5–11.
E. Sandier and S. Serfaty (2007), *Vortices in the Magnetic Ginzburg-Landau Model*, Progr. Nonlinear Differential Equations Appl. 70, Birkhäuser, Boston.
C.E. Shannon (1948), *A Mathematical Theory of Communication*, Bell System Tech. J., 27, pp. 379–423.
S. Smale (2000), *Mathematical problems for the next century*, in Mathematics: Frontiers and Perspectives, V. Arnold, M. Aliyah, P. Lax, and B. Mazur, eds., AMS, Providence, RI, pp. 271–294.
H.A.M. Snelders (1976), *A.M. Meyer's experiments with floating magnets and their use in the atomic theories of matter*, Ann. Sci., 33, pp. 67–80.
E.B. Sonin (1987), *Vortex oscillations and hydrodynamics of rotating superfluids*, Rev. Modern Phys., 59, pp. 87–155.
R. Szeliski, D. Tonnesen, and D. Terzopoulos (1993), *Modeling surfaces of arbitrary topology with dynamic particles*, in Proceedings of the 1993 IEEE Conference on Computer Vision and Pattern Recognition (CVPR '93), IEEE, pp. 82–87.
P.M.L. Tammes (1930), *On the origin of number and arrangements of the places of exit on the surface of pollen-grains*, Recl. Trav. Bot. Neerl., 27, pp. 1–84.
J.J. Thomson (1904), *On the structure of the atom*, Philos. Mag., 7, pp. 237–265.
W. Thomson (1878), *Floating magnets [illustrating vortex systems]*, Nature, 18, pp. 13–14.
W. Thomson (1867), *On vortex atoms*, Phil. Mag., 34, pp. 15–24.
W. Thomson (1887), *On the propagation of laminar motion through a turbulently moving inviscid fluid*, in William Thomson, Mathematical and Physical Papers, Vol. 4., 1882–1911, Cambridge University Press, Cambridge, UK, 1910, pp. 308–320
V.K. Tkachenko (1966a), *On vortex lattices*, Soviet Phys. JETP, 22, pp. 1282–1286.
V.K. Tkachenko (1966b), *Stability of vortex lattices*, Soviet Phys. JETP, 23, pp. 1049–1056.
L.N. Trefethen and D. Bau III (1997), *Numerical Linear Algebra*, SIAM, Philadelphia.
D.J. Wales and S. Ulker (2006), *Structure and dynamics of spherical crystals characterized for the Thomson problem*, Phys. Rev. B, 74, article 212101.
R.B. Warder and W.P. Shipley (1888), *Floating magnets*, Amer. J. Sci., 20, pp. 285–288.
L.T. Wille (1986), *Searching potential energy surfaces by simulated annealing*, Letters to Nature (London), 324, pp. 46–48.
A. P. Witkin and P.S. Heckbert (1994), *Using particles to sample and control implicit surfaces*, in Proceedings of the 21st Annual Conference on Computer Graphics and Interactive Techniques, pp. 269–277.
R.W. Wood (1898), *Equilibrium figures formed by floating magnets*, Philos. Mag., 46, pp. 162–164.
E.J. Yarmchuck, M.J.V. Gordon, and R. Packard (1979), *Observation of stationary vortex arrays in rotating superfluid helium*, Phys. Rev. Lett., 43, pp. 214–217. (See also Phys. Today, 32 (1979), p. 21.)
Y. Zhang, W. Bao, and Q. Du (2007), *The dynamics and interaction of quantized vortices in the Ginzburg–Landau–Schrödinger equation*, SIAM J. Appl. Math., 67, pp. 1740–1775.